Stem Cell Reports
Article
ISSCR
OPEN ACCESS

p19^{INK4d} Controls Hematopoietic Stem Cells in a Cell-Autonomous Manner during Genotoxic Stress and through the Microenvironment during Aging

Morgane Hilpert,[1,2,3,4] Céline Legrand,[1,2,3] Dominique Bluteau,[1,2,3,5] Natalie Balayn,[1,2,3] Aline Betems,[1,2,3] Olivier Bluteau,[1,2,3] Jean-Luc Villeval,[1,2,3] Fawzia Louache,[1,2,3] Patrick Gonin,[2,3] Najet Debili,[1,2,3] Isabelle Plo,[1,2,3] William Vainchenker,[1,2,3] Laure Gilles,[1,2,3,6] and Hana Raslova[1,2,3,6,*]

[1]Institut National de la Santé et de la Recherche Médicale, U1009, Equipe labellisée Ligue Nationale contre le Cancer, 114 rue Edouard Vaillant, 94805 Villejuif, France
[2]University Paris Sud, 114, rue Edouard Vaillant, 94805 Villejuif, France
[3]Gustave Roussy, IFR54, 114, rue Edouard Vaillant, 94805 Villejuif, France
[4]University Paris Diderot, 5 rue Thomas-Mann, 75205 Paris, France
[5]Ecole Pratique des Hautes Etudes, 4-14 rue Ferrus, 75014 Paris, France
[6]Co-senior author
*Correspondence: hraslova@igr.fr
http://dx.doi.org/10.1016/j.stemcr.2014.10.005

SUMMARY

Hematopoietic stem cells (HSCs) are characterized by the capacity for self-renewal and the ability to reconstitute the entire hematopoietic compartment. Thrombopoietin maintains adult HSCs in a quiescent state through the induction of cell cycle inhibitors p57^{Kip2} and p19^{INK4d}. Using the *p19$^{INK4d-/-}$* mouse model, we investigated the role of p19^{INK4d} in basal and stress-induced hematopoiesis. We demonstrate that p19^{INK4d} is involved in the regulation of HSC quiescence by inhibition of the G0/G1 cell cycle transition. Under genotoxic stress conditions, the absence of p19^{INK4d} in HSCs leads to accelerated cell cycle exit, accumulation of DNA double-strand breaks, and apoptosis when cells progress to the S/G2-M stages of the cell cycle. Moreover, p19^{INK4d} controls the HSC microenvironment through negative regulation of megakaryopoiesis. Deletion of *p19^{INK4d}* results in megakaryocyte hyperproliferation and increased transforming growth factor β1 secretion. This leads to fibrosis in the bone marrow and spleen, followed by loss of HSCs during aging.

INTRODUCTION

Hematopoietic stem cells (HSCs) possess the capacity for self-renewal and multilineage differentiation that underlies the maintenance and reconstitution of the entire hematopoietic compartment. In the bone marrow (BM), the majority of HSCs remain quiescent in the G0 phase of the cell cycle. Upon exposure to stress, the number of mature cells in the blood circulation is reduced, causing quiescent HSCs to enter the cell cycle and replenish the hematopoietic system.

Accumulating evidence has demonstrated that quiescence is an active process regulated by intrinsic factors, including numerous transcription factors, as well as environmental cues, including the Notch, Wnt, and Sonic hedgehog signaling pathways. Cytokines also play a major role in regulating the HSC cell cycle. For example, thrombopoietin (TPO), the primary regulator of megakaryocyte (MK) differentiation, is required for the maintenance of adult HSC quiescence, via induction of the cell cycle inhibitors, p57^{Kip2} and p19^{INK4d} (Qian et al., 2007; Yoshihara et al., 2007). TGF-β1 can also enforce HSC quiescence by inducing p57^{Kip2} expression (Scandura et al., 2004; Yamazaki and Nakauchi, 2009).

Cyclin-dependent kinase inhibitors (CDKIs) directly control the cell cycle by inhibiting cell cycle entry. They are divided into two groups: the INK4 family and the Cip/Kip family.

Cip/Kip proteins are expressed at higher levels in HSCs than in progenitor cells (Passegué et al., 2005). The role of p21^{Cip1} in HSCs is restricted to cell cycle regulation under stress conditions (van Os et al., 2007). p27^{Kip1} deficiency does not affect HSC numbers or HSC self-renewal, but alters the proliferation of progenitor cells (Cheng et al., 2000a). p57^{Kip2} is an important regulator of hematopoiesis in the aorta gonads mesonephros region, where HSCs emerge (Mascarenhas et al., 2009). Inducible loss of *p57^{Kip2}* in hematopoietic cells has demonstrated the critical role of this CDKI in the maintenance of HSC quiescence (Matsumoto et al., 2011).

More recent studies have implicated INK4 members in the control of HSC functions. p16^{INK4a} expression is repressed by EZH1 in young animals (Hidalgo et al., 2012). Its expression increases with age, contributing to the decreased self-renewal, homing, and repopulating activities of HSCs in response to stress (Janzen et al., 2006). However, the role of p16^{INK4a} in regulating steady-state HSC aging in vivo appears to be less important (Attema et al., 2009).

p18^{INK4c} is also involved in the senescence of HSCs. In its absence, the number of cycling HSCs increases, although the overall self-renewal capacity of the HSC compartment

remains unchanged (Yuan et al., 2006). In a sense, *p18*^{INK4c} deletion mimics HSC aging, and it may, paradoxically, have an opposite role to p16^{INK4a} and p21^{Cip1}.

Prior evidence for the importance of p19^{INK4d} in HSC cell cycle regulation was reported using the *Thpo*$^{-/-}$ mouse model. These mice exhibit a significant decrease in HSC numbers that correlates with decreased expression of p19^{INK4d} and p57^{Kip2} (Qian et al., 2007; Yoshihara et al., 2007). p19^{INK4d} plays a role in the development of the cerebral cortex (Zindy et al., 1999), controls mouse spermatogenesis (Zindy et al., 2001), and is involved in macrophage differentiation (Adachi et al., 1997). We previously demonstrated that by linking endomitotic arrest and terminal maturation p19^{INK4d} is implicated in megakaryopoiesis (Gilles et al., 2008). In addition to its role in cell cycle and differentiation, in neuroblastoma cells, p19^{INK4d} is also important for DNA repair and resistance to apoptosis in response to diverse forms of genotoxic stress (Ceruti et al., 2009). Interestingly, sensory hair cells lacking p19^{INK4d} aberrantly re-enter the cell cycle and subsequently undergo apoptosis. This supports the notion that p19^{INK4d} is essential for maintenance of their postmitotic state (Chen et al., 2003) and that p19^{INK4d} therefore acts as an antiapoptotic regulator.

Although a number of studies suggest that p19^{INK4d} is implicated in HSC biology, its precise role remains unclear. Using a *p19*$^{INK4d-/-}$ mouse model, we demonstrate that p19^{INK4d} is involved in the regulation of HSC quiescence. Under conditions of genotoxic stress, the absence of p19^{INK4d} leads to HSC apoptosis during the S/G2-M phases of the cell cycle. We also report that p19^{INK4d} participates in control of the HSC microenvironment during aging, as its absence results in BM and spleen fibrosis, and loss of HSCs.

RESULTS

Loss of p19^{INK4d} Affects HSC Numbers

The expression profile of different CDKIs has previously been reported in C57BL/6 mice (Passegué et al., 2005). Since the *p19*$^{INK4d-/-}$ mice in this study are in a mixed C57BL/6 × Sv129j genetic background, we first compared the expression level of all CDKIs in mice with a mixed genetic background with that of pure C57BL/6 mice. In long-term (LT) HSCs, purified as the CD48^{-}CD150^{+} (SLAM) cell subpopulation of primitive Lin^{-}SCA1^{+}C-KIT^{+} (LSK) BM cells, *p19*^{INK4d} transcript levels were similar in both genetic backgrounds. Slight differences in transcript levels were observed in both the immature and more mature progenitor populations (Figure 1A). The levels of other CDKIs expressed during hematopoiesis were similar between C57BL/6 and C57BL/6 × Sv129j mice (Figures S1A–S1D available online). We observed relatively high levels of *p27*^{Kip1} and *p19*^{INK4d} transcripts in SLAM cells compared with *p18*^{INK4c}, *p21*^{Cip1} and *p57*^{Kip2}, suggesting that p27^{Kip1} and p19^{INK4d} have important roles in quiescent HSCs.

To investigate the function of p19^{INK4d}, we first analyzed the total number of BM cells in 8- to 10-week-old mice. A 1.23-fold increase in total BM cells was observed in *p19*$^{INK4d-/-}$ mice (Figure 1B). No significant difference was observed in the absolute number of LSK cells (Figures 1C and 1D). In contrast, a significant decrease (1.75-fold) in the absolute number of SLAM cells (Figures 1C and 1E) was observed for *p19*$^{INK4d-/-}$ mice. This result was confirmed by characterizing the LSK side population (SP). The upper SP is biased toward lymphoid differentiation and the lower SP toward myeloid differentiation (Challen et al., 2010) (Figure 1F). We confirmed a 2.1-fold decrease in HSC numbers (total SP population) (Figure 1G). No difference was observed in the lymphoid-biased HSC population (Figure 1H), although myeloid-biased HSCs were decreased 4.1-fold in *p19*$^{INK4d-/-}$ mice (Figure 1I).

p19^{INK4d} Is Involved in the Regulation of HSC Quiescence by Inhibition of the G0/G1 Transition

To study the role of p19^{INK4d} in the cell cycle, we stained LSK and SLAM cells with anti-Ki-67 and Hoechst (Figure 2A). A significant acceleration in the G0/G1 transition was observed in *p19*$^{INK4d-/-}$ mice, without any significant change in the S/G2-M phases (Figures 2B and 2C). Using LT bromodeoxyuridine (BrdU) incorporation (Figure 2D), a 1.3- and 1.9-fold decrease in the percentage of BrdU-positive cells was observed in LSK and SLAM cells at day (D) 8. The effect on BrdU incorporation was even more pronounced at D11 and D21, particularly for SLAM cells (Figures 2E and 2F). These experiments revealed an increased G0/G1 transition (Figure 2C), with a decreased progression to S/G2-M phases for *p19*$^{INK4d-/-}$ HSCs. Since no increase in the number of LSK cells was detected, we investigated whether the absence of p19^{INK4d} was associated with apoptosis in cycling LSK and SLAM cells (Figure 2G). We observed a significant increase in the percentage of annexin-V^{+}/BrdU^{+} cells in the LSK population at D11 (1.4-fold) and D21 (1.6-fold) in *p19*$^{INK4d-/-}$ mice (Figure 2H), which was even more pronounced in the SLAM population (3.5- and 1.7-fold at D11 and D21, respectively; Figure 2I). These results suggest that p19^{INK4d} protects immature progenitors and, to an even greater extent, HSCs from apoptosis in the S/G2-M phases of the cell cycle.

p19^{INK4d} Plays a Crucial Role in Stress-Induced Hematopoiesis

To investigate the consequence of this increased HSC cell cycle progression that is followed by enhanced apoptosis in *p19*$^{INK4d-/-}$ mice during hematopoietic stress,

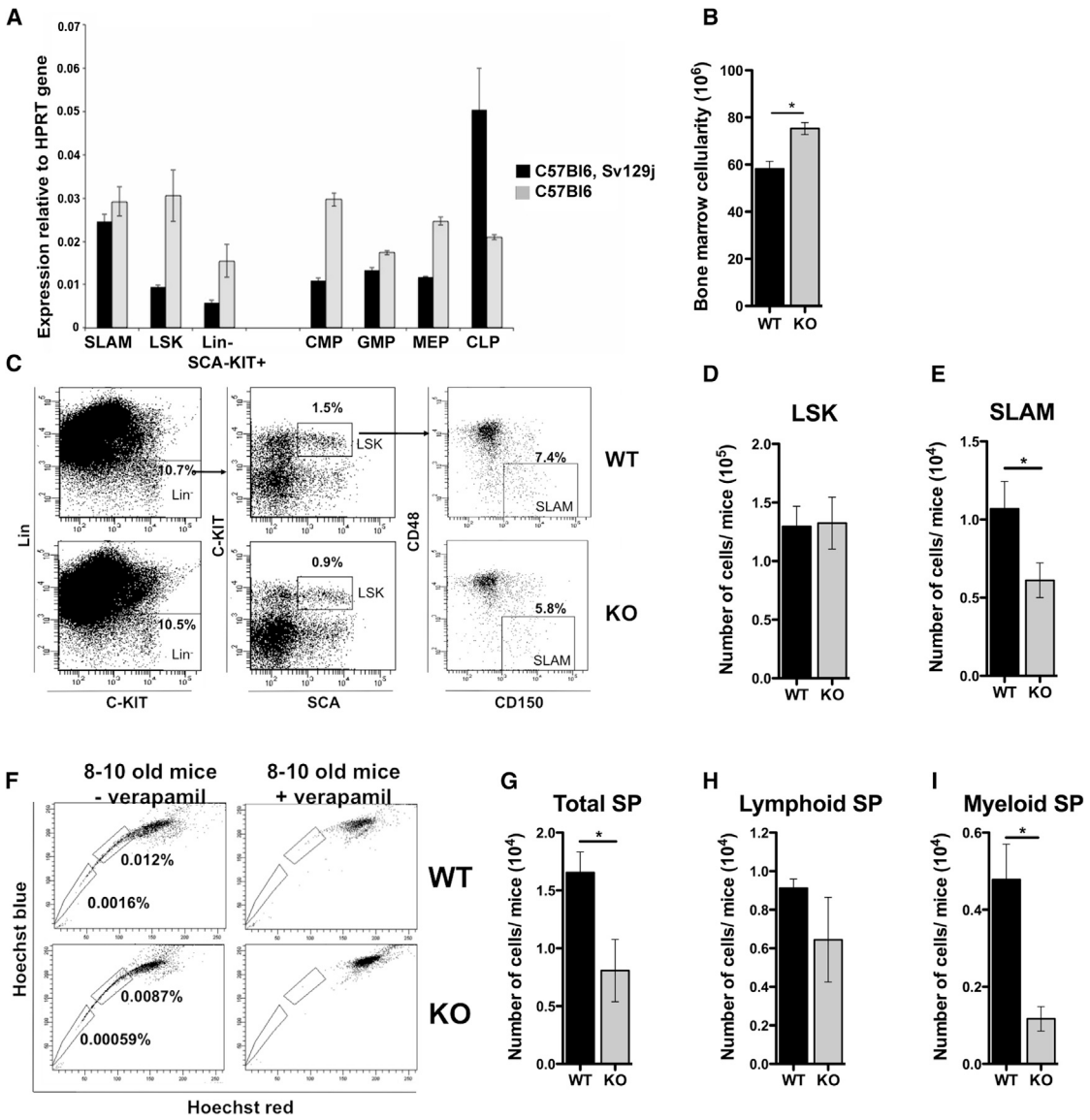

Figure 1. $p19^{INK4d-/-}$ Mice Exhibit a Defect in the HSC Compartment

(A) mRNA expression level of $p19^{INK4d}$ in different populations of C57BL/6 and C57BL/6-Sv129j mice: SLAM ($Lin^-SCA1^+C\text{-}KIT^+CD48^-CD150^+$), LSK, myeloid progenitors ($Lin^-SCA1^-C\text{-}KIT^+$), CLP ($Lin^-SCA1^{low}C\text{-}KIT^{low}CD127^+THY\text{-}1^-$), CMP ($Lin^-SCA1^-C\text{-}KIT^+FC\gamma R^-CD34^+$), GMP ($Lin^-SCA1^-C\text{-}KITt^+FC\gamma R^+CD34^+$), and MEP ($Lin^-SCA1^-C\text{-}KIT^+FC\gamma R^-CD34^-$). Each population represents a pool derived from 10 mice. Data are normalized to *HPRT* transcript levels and represent the mean ± SEM of triplicates.

(B) BM cellularity (n = 10).

(C–E) Immunophenotype (C) and number of LSK (D) and SLAM (E) cells (n = 8).

(F–I) Immunophenotype (F) and number of total SP (G), lymphoid SP (H), and myeloid SP (I) populations (n = 4).

Mice that were 8 to 10 weeks old were used. KO, $p19^{INK4d-/-}$. Data represent mean ± SEM. *p < 0.05, **p < 0.01, unpaired t test. See also Figure S1.

we examined the effect of stress-inducing compounds, 5-fluorouracil (5-FU), hydroxyurea (HU), and menadione.

$p19^{INK4d-/-}$ mice exhibited a markedly increased mortality after weekly injections of 5-FU (Figure 3A). To confirm that the increased mortality is related to a more rapid exhaustion of $p19^{INK4d-/-}$ HSCs as a consequence of the enhanced G0/G1 transition that is followed by apoptosis, we analyzed the cell cycle of WT and $p19^{INK4d-/-}$ HSC/Ps 4 days after 5-FU injection (Figure 3B). As expected, we observed a substantial decrease in quiescent $p19^{INK4d-/-}$

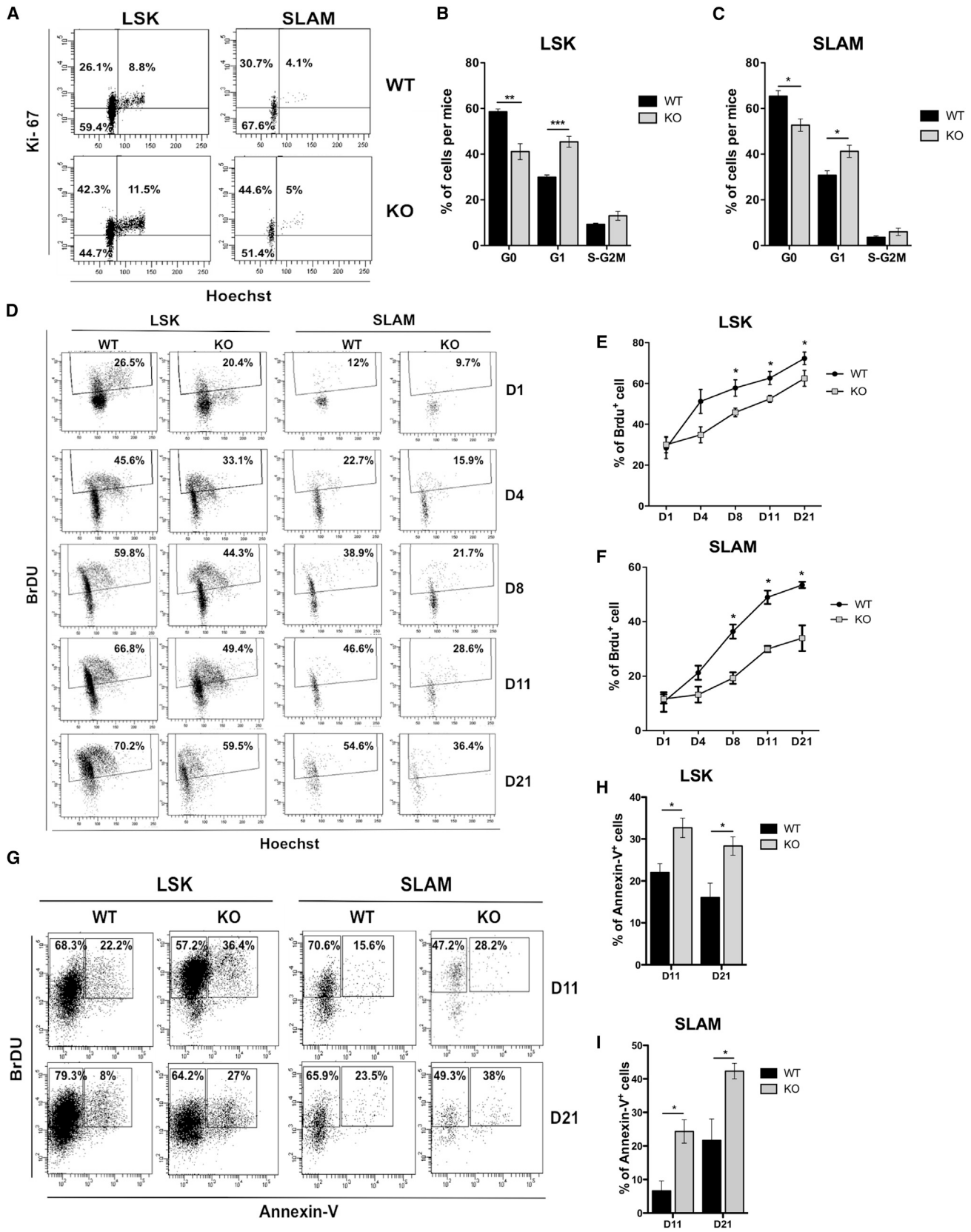

(legend on next page)

LSK (2.6-fold) and SLAM (11.6-fold) cell numbers, with a concomitant increase in G1 phase cells, whereas no differences in the number of cells in S/G2-M phases were observed (Figures 3C and 3D).

To investigate the role of p19^{INK4d} under other stress conditions, we treated Lin$^-$ cells with menadione and measured the endogenous levels of reactive oxygen species (ROS). ROS levels were identical in WT and *p19$^{INK4d-/-}$* LSK and SLAM cells under basal conditions (Figures 3E–3G). Following menadione treatment, ROS levels were greatly increased in LSK and SLAM cells of both WT and *p19$^{INK4d-/-}$* mice; however, levels were significantly higher in the *p19$^{INK4d-/-}$* genetic background (1.7- and 2.2-fold increase in LSK and SLAM populations, respectively) (Figures 3E–3G). In accordance with the fact that high ROS levels increase DNA damage and subsequently induce apoptosis, we observed a 1.75- and 1.8-fold increase in annexin-V$^+$ cells in *p19$^{INK4d-/-}$* LSK and SLAM populations, respectively (Figures 3H and 3I). Analysis of the level of phospho-H2AX (P-H2AX), a biomarker of DNA double-strand breaks (DNA-DSBs), revealed that in comparison to WT cells, the number of large P-H2AX foci in *p19$^{INK4d-/-}$* LSK cells was already higher prior to stress induction and further increased following the induction of oxidative stress (Figures 3J and 3K).

To determine the role of p19^{INK4d} during another type of stress, we treated WT and *p19$^{INK4d-/-}$* mice with HU for 3 consecutive days and subsequently analyzed cell cycle and apoptosis in the LSK and SLAM populations (Figures S2A–S2D). As expected, a slight increase in the percentage of S phase (Figures S2A and S2B) and apoptotic (Figure S2C) cells was observed after HU treatment of both WT and *p19$^{INK4d-/-}$* mice. However, no difference in the percentage of annexin-V$^+$ LSK and SLAM cells was observed between WT and *p19$^{INK4d-/-}$* mice after HU treatment (Figure S2D). Together, these results suggest that p19^{INK4d} is predominantly involved in the response to genotoxic and oxidative stresses, but not to replicative stress induced by HU treatment.

Finally, to determine whether the effect of 5-FU on HSCs was cell autonomous or related to the microenvironment, we transplanted either *p19$^{INK4d-/-}$* or WT hematopoietic Lin$^-$ cells into lethally irradiated recipients of both genetic backgrounds in order to obtain chimeric mice. One month after hematopoietic reconstitution, 5-FU was injected twice and mortality was monitored as described previously. As expected, all *p19$^{INK4d-/-}$*/*p19$^{INK4d-/-}$* and *p19$^{INK4d-/-}$*/WT mice died after treatment with 5-FU (150 mg/kg), while survival of WT/WT mice was higher, in the range of 20%–35%. Surprisingly, all chimeric WT/*p19$^{INK4d-/-}$* mice also died, but with delayed kinetics compared with the *p19$^{INK4d-/-}$*/*p19$^{INK4d-/-}$* mice, suggestive of a defect in the hematopoietic microenvironment of *p19$^{INK4d-/-}$* mice (Figure 3L).

To differentiate the cell-autonomous and environmental effects of p19^{INK4d} on the cell cycle (Figures 3M and 3N) and apoptosis (Figures 3O and 3P) following induction of stress, a lower dose of 5-FU (50 mg/kg) was injected into the chimeric mice 2 months after reconstitution. Within 48 hr, a more rapid exhaustion of quiescent *p19$^{INK4d-/-}$* LSK (Figure 3M) and SLAM (Figure 3N) cells was observed compared with WT cells, regardless of the genetic background of the recipient mice. This cell cycle re-entry was accompanied by an increased percentage of *p19$^{INK4d-/-}$* cells in G1 and S/G2-M phases (Figures 3M, 3N, S2E, and S2F). Increased apoptosis was also detected in both LSK (Figure 3O) and SLAM (Figure 3P) *p19$^{INK4d-/-}$* cells compared with WT cells, regardless of the genetic environment. These results clearly demonstrate the intrinsic role of p19^{INK4d} in maintaining HSC quiescence and in protecting cells from apoptosis following genotoxic stress.

In conclusion, under conditions of stress, p19^{INK4d} loss leads to enhanced cell cycle progression, accumulation of ROS, and increased DNA damage and apoptotic cell death in a cell autonomous manner.

p19$^{INK4d-/-}$ BM Cells Exhibit High Reconstitutive Activity, but the *p19$^{INK4d-/-}$* Stroma Displays a Defective HSC Supportive Activity

To better assess the defect in the microenvironment, we tested the reconstitutive capacities of *p19$^{INK4d-/-}$* BM Lin$^-$ cells in competitive transplantation assays (Figure 4A).

Figure 2. Absence of p19^{INK4d} Leads to Accelerated Exit of HSCs from Quiescence and Increased Apoptosis in S/G2-M Cell Cycle Phases

(A–C) Cell cycle analysis by Ki-67/Hoechst costaining. Immunophenotype (A) and frequencies of cell cycle phases in LSK (B) and SLAM (C) populations (n = 4) are shown.

(D–F) In vivo cell proliferation assays post-BrdU administration in mice by BrdU/Hoechst costaining. Immunophenotype (D) and frequencies of cell cycle phases in LSK (E) and SLAM (F) populations are shown. One of three independent experiments with similar results is presented. For each experiment, three mice were analyzed per point.

(G–I) Apoptosis assessment at D11 or D21 post-BrdU administration. Immunophenotype (G) and frequencies of annexin-V$^+$ cells in LSK (H) and SLAM (I) populations are shown. One of two independent experiments with similar results is presented. For each experiment, four mice were analyzed per data point.

Mice that were 8 to 10 weeks old were used. KO, *p19$^{INK4d-/-}$*. Data represent mean ± SEM. *p < 0.05, **p < 0.01, ***p < 0.001, unpaired t test.

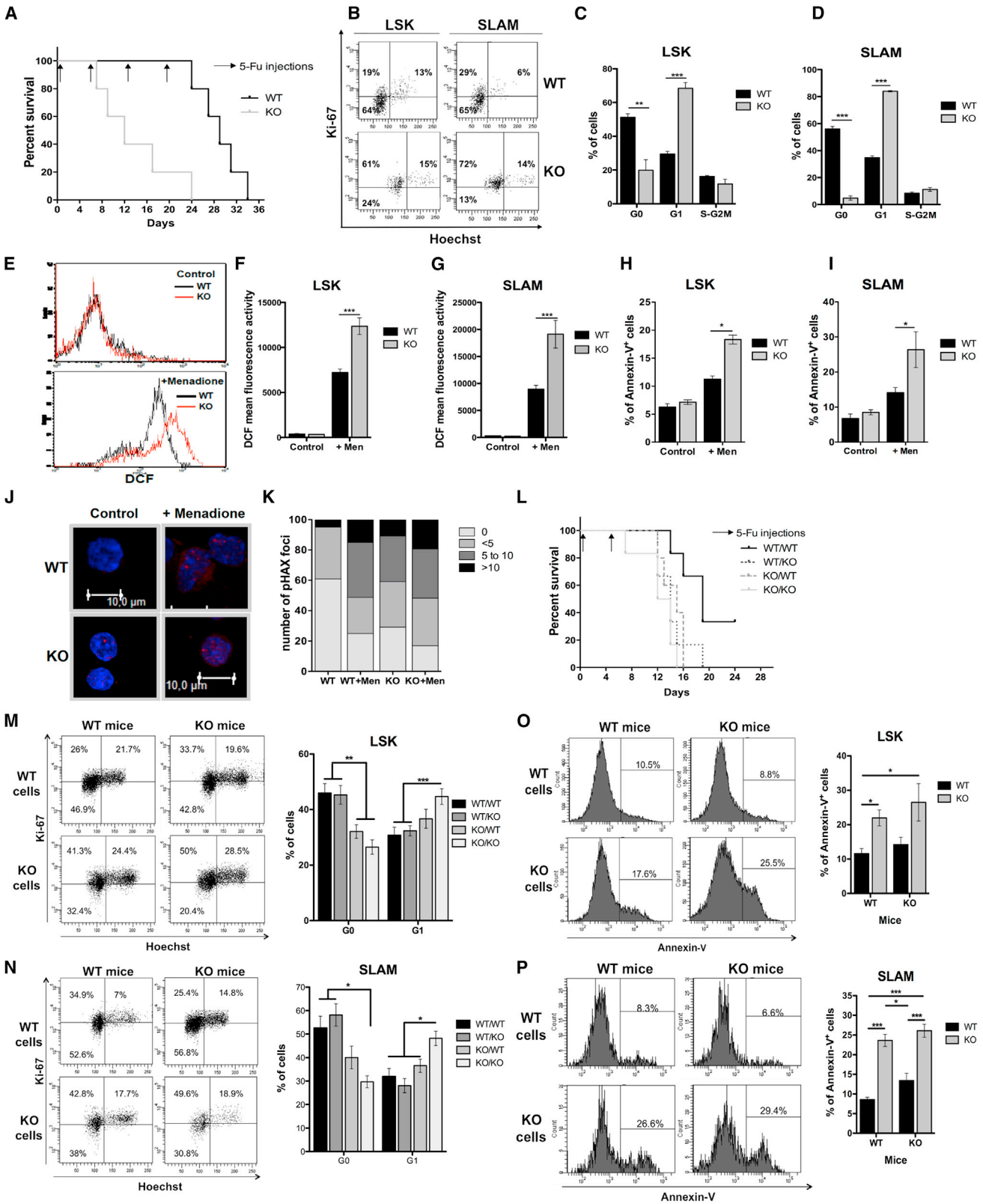

(legend on next page)

At 15-weeks postengraftment, the increase in the fraction of *p19$^{INK4d-/-}$* SLAM, LSK, and myeloid cells was 9.9-, 2.26-, and 2.75-fold, respectively (Figure 4B). This result strongly supports the hypothesis that HSCs, which are less numerous in *p19$^{INK4d-/-}$* mice, exhibit a higher repopulating capacity than WT HSCs when injected into WT recipients. This paradoxical result further implies that the BM microenvironment is defective in *p19$^{INK4d-/-}$* mice. To test this hypothesis, adherent stromal BM cells were isolated from *p19$^{INK4d-/-}$* and WT mice, and their capacity to maintain LT culture initiating cells (LTC-ICs) was assessed (Figure 4C). WT and *p19$^{INK4d-/-}$* cells exhibited a 2.3- and 2.6-fold reduction, respectively, in the number of LTC-ICs on the *p19$^{INK4d-/-}$* stroma compared with the WT stroma (Figure 4D). No marked difference in LTC-IC content was observed between WT and *p19$^{INK4d-/-}$* mice, regardless of the stroma used. This demonstrates that p19^{INK4d} is also required for maintenance of the hematopoietic function of the BM microenvironment. To confirm this result in vivo, reconstitution of lethally irradiated WT or *p19$^{INK4d-/-}$* mice with WT or *p19$^{INK4d-/-}$* donor total BM cells was performed. In this assay, WT and *p19$^{INK4d-/-}$* BM cells have similar irradiation protective properties in WT recipients. However, a defect in survival was observed in *p19$^{INK4d-/-}$* recipient mice transplanted with WT BM, and this occurred to an even greater extent with *p19$^{INK4d-/-}$* BM cells (Figure 4E). These results clearly demonstrate an important role for p19^{INK4d} in the regulation of both the BM environment and HSCs.

Hematopoietic tissue maintenance under homeostatic conditions is controlled by a large number of soluble cytokines, growth factors, cell-cell interaction molecules, and extracellular matrix components. We determined the levels of two pivotal growth factors in fluid extracted from the BM of WT and *p19$^{INK4d-/-}$* mice that exert positive (TPO) or negative (transforming growth factor β1 [TGF-β1]) regulation HSC numbers. No differences in TPO levels were observed, while TGF-β1 levels were significantly increased in *p19$^{INK4d-/-}$* mice. The levels of several other inflammatory cytokines were also significantly increased in *p19$^{INK4d-/-}$* mice (Figure 4F).

A Defect in the MK Lineage Is Involved in the Defective Microenvironment and Leads to Progressive Fibrosis and Osteosclerosis in *p19$^{INK4d-/-}$* Mice

MKs play an important role in the BM niche via secretion of cytokines such as TGF-β1 and by cell-cell interactions. This led us to perform a detailed study of the MK lineage in *p19$^{INK4d-/-}$* mice during aging, as this is a biological process that is known to modify HSC properties. While no differences were observed in MK-P numbers of 8- to 10-week-old mice compared with WT mice, the frequency of MK-Ps at 20–25 weeks was increased 2.3-fold in the BM and 6.1-fold in the spleen of *p19$^{INK4d-/-}$* mice (Figures 5A and 5B). In contrast, no differences were observed for all other BM myeloid progenitors during aging (Figures S3A and S3B). In peripheral blood, a significant increase in red blood cells and lymphocytes detected in WT mice was not observed in *p19$^{INK4d-/-}$* mice (Figures S3C–S3F). In contrast, the slight increase in platelet counts observed in young *p19$^{INK4d-/-}$* animals was more pronounced (1.35-fold) in *p19$^{INK4d-/-}$* mice that were older than 91 weeks (Figure S3F).

To determine whether the increased MK-P number has consequences on the total MK cell population, we performed a histological examination of BM and spleen from mice of different ages. Accumulation of clustered, polylobulated MKs (Figure S3G) in the BM and spreading of the red pulp (Figure S3H) in the spleen of *p19$^{INK4d-/-}$* mice were detected during aging. von Willebrand factor

Figure 3. Hematopoietic Stress in *p19$^{INK4d-/-}$* Mice Leads to a Defect in Survival due to Increased HSC Exhaustion and Apoptosis

(A) Survival rate of mice injected weekly with 5-FU. One of two independent experiments with similar results is presented. For each experiment, five mice were injected.

(B–D) Cell cycle analysis by Ki-67/Hoechst costaining four days after 5-FU injection. Immunophenotype (B) and cell cycle distribution in LSK (C) and SLAM (D) populations are shown (n = 4).

(E–G) Immunophenotype of DCF staining (E) and DCF mean fluorescence in LSK (F) and SLAM (G) populations before and after oxidative stress induction by menadione (n = 4).

(H and I) Annexin-V staining before and after oxidative stress induction by menadione in LSK (H) and SLAM (I) populations (n = 4).

(J and K) P-H2AX staining in LSK cells before and after oxidative stress induction with menadione. Representative pictures (J) are shown. Nuclei are stained with DAPI (blue) and DNA-DSBs with an anti-P-H2AX antibody (red). (K) The number of P-H2AX foci per 100 LSK cells.

(L) Survival rate of sublethally irradiated mice reconstituted with 2 × 10^5 Lin$^-$ cells and injected with 5-FU 1 month after reconstitution. One of two independent experiments with similar results is presented. For each experiment, six mice were injected.

(M and N) The distribution of cells in the cell cycle was determined by Ki-67/Hoechst costaining 2 days after 5-FU injection. Immunophenotype and frequencies of cell cycle phases in LSK (M) and SLAM (N) populations in 2-month-old transplanted lethally irradiated mice are shown (n = 6).

(O and P) Annexin-V staining two days after 5-FU treatment in LSK (O) and SLAM (P) populations (n = 4).

Mice that were 8 to 10 weeks old were used. KO, *p19$^{INK4d-/-}$*. Data represent mean ± SEM. *p < 0.05, **p < 0.01, ***p < 0.001, unpaired t test. See also Figure S2.

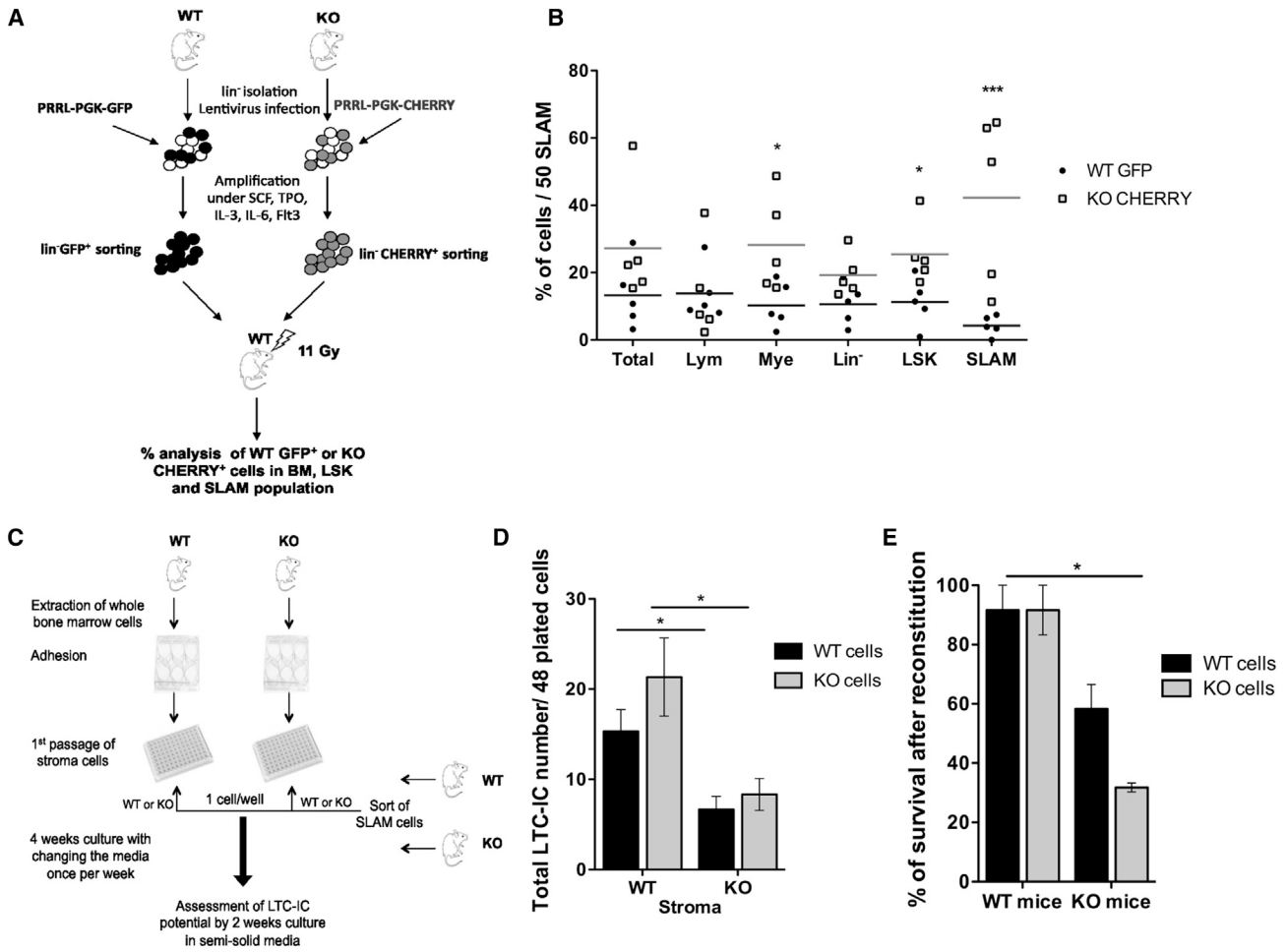

(legend on next page)

(vWF) staining of BM (Figures 5C and 5E) and spleen (Figures 5D and 5F) revealed that the total MK number increased progressively with age in BM of WT mice. However, this increase occurred more rapidly in the BM of *p19$^{INK4d-/-}$* mice, reaching a plateau at 20–25 weeks (3.4-fold increase) (Figure 5C). A 6.2-fold increase in the number of MKs was observed in the spleen of aged *19$^{INK4d-/-}$* mice, whereas MK numbers remained constant in the spleen of aged WT mice (Figure 5D). Since p19^{INK4d} regulates MK ploidization arrest (Gilles et al., 2008), we next investigated MK ploidy (Figure 5G). Regardless of age, the modal ploidy level remained 64N in *p19$^{INK4d-/-}$* mice compared with 16N for WT MKs (Figure 5H). However, a progressive increase in the proliferative 2N/4N MK population was noted in BM during aging (Figure 5I). Overall these results demonstrate that p19^{INK4d} is involved not only in the arrest of ploidization, but also in regulation of the cell cycle in MK-Ps, thereby explaining the increase in MKs with age.

To determine whether the increase in MKs observed with aging in *p19$^{INK4d-/-}$* mice was due exclusively to an intrinsic role of p19^{INK4d}, MK-Ps, and MKs were quantified in 8-month-old chimeric mice. A significant increase in the number of MK-Ps in both BM (Figure 5J) and spleen (Figure 5K) was detected when WT or *p19$^{INK4d-/-}$* recipient mice were reconstituted with *p19$^{INK4d-/-}$* cells. The same profile was observed for MK numbers in both BM (Figure 5L) and spleen (Figure 5M). These results indicate that MK amplification is due to an intrinsic role of p19^{INK4d}.

The loss of p19^{INK4d} therefore mimics hematopoietic stress, which is normally associated with hematopoietic development in the spleen and induction of splenomegaly. Accordingly, the spleen size did not change for WT mice during aging, whereas a 1.4-fold increase in spleen size for *p19$^{INK4d-/-}$* mice was already observed at 8–10 weeks of age. This effect became more pronounced as a function of age (Figure 6A) and was associated with a parallel increase in spleen cellularity (Figure 6B). To determine the role of the microenvironment in the splenomegaly, spleen weights were determined for 8-month-old chimeric mice. A significant increase in spleen weight was detected when WT and *p19$^{INK4d-/-}$* recipient mice were reconstituted with *p19$^{INK4d-/-}$* cells (Figure 6C), suggesting an intrinsic role of p19^{INK4d} in extramedullary hematopoiesis.

An enhanced MK mass is typically associated with increased TGF-β1 secretion. The levels of active and latent TGF-β1 in the extracellular fluids from BM and spleen directly paralleled MK numbers in BM and spleen during aging (Figures 6D–6G). Nonetheless, the level of active TGFβ1 increased in the BM of *p19$^{INK4d-/-}$* mice until 20–25 weeks of age, after which it decreased again (Figure 6D). In the spleen, a strong increase was also already observed at 20–25 weeks (Figure 6F). The presence of active TGF-β1 in tissues is usually associated with fibrosis. Increased reticulin fiber deposition was observed during aging in *p19$^{INK4d-/-}$* mice. In mice older than 91 weeks, fibrosis was detected in the spleens of all *p19$^{INK4d-/-}$* mice (Figure 6H) and in the BM of 20% of mice (Figure S4A). Osteosclerosis could also be observed in these mice (Figure S4B, upper panels). Consistent with the changes observed in myelofibrosis, we also detected an increase in circulating myeloid (Lin$^-$Sca1$^-$Kit$^+$) progenitors (Figure 6I) and LSK cells (Figure 6J) in older mice.

To investigate whether fibrosis was a consequence of abnormal hematopoiesis, we transplanted a pool of total BM and spleen cells from *p19$^{INK4d-/-}$* mice with myelofibrosis and a spleen weight of 4 g into lethally irradiated WT recipients. At 6 weeks posttransplantation, splenomegaly was detected in primary recipients and in a less pronounced manner also in secondary recipients (Figure S4C). No osteosclerosis or fibrosis of the BM was observed (Figure S4B). However, fibrosis was detected in the spleen of both primary and secondary recipients, and this correlated with the increased MK numbers (Figure S4D).

These results indicate that the disease is transplantable and that it originates in the hematopoietic system.

p19^{INK4d} Regulates HSC Number during Aging

p19^{INK4d} loss increased MK mass and resulted in elevated TGF-β1 secretion and fibrosis during aging. The TGF-β1 pathway has previously been reported to regulate the

Figure 4. The Hematopoietic Supportive Function of the Microenvironment Is Altered by p19^{INK4d} Loss

(A and B) Competitive engraftment between Lin$^-$GFP$^+$WT cells and Lin$^-$CHERRY$^+$KO cells in recipient lethally irradiated WT mice. The experimental protocol (A) and percentage of WT GFP$^+$ and KO CHERRY$^+$ BM-derived cells (B) are shown in the following hematopoietic populations: myeloid (GR1$^+$CD11b$^+$), T lymphoid (CD3$^+$), Lin$^-$, LSK, and SLAM per 50 transplanted SLAM cells at 15 weeks postengraftment. Each dot represents data from a single mouse (n = 5).

(C and D) LTC-IC growth of WT and KO SLAM cells on WT and KO stroma. Experimental protocol (C) and number of LTC-IC/48 plated cells (D) (n = 3) are shown.

(E) Potential of WT and KO HSC engraftment in WT and KO mice evaluated as the percentage of survival after reconstitution. One of two independent experiments with similar results is presented (n = 6).

(F) Level of different cytokines/chemokines in BM supernatants, (n = 5) for TPO and TGF-β1, (n = 3) for interferon γ (IFN-γ), interleukin 1α (IL-1α), IL-16, IL-3, IL-10, IL-23, granulomonocyte stem call factor, and macrophage inflammatory protein 1α (MIP-1α) and MIP-1β. Mice that were 8 to 10 weeks old mice were used. KO, *p19$^{INK4d-/-}$*. Data represent mean ± SEM. *p < 0.05, **p < 0.01, unpaired t test.

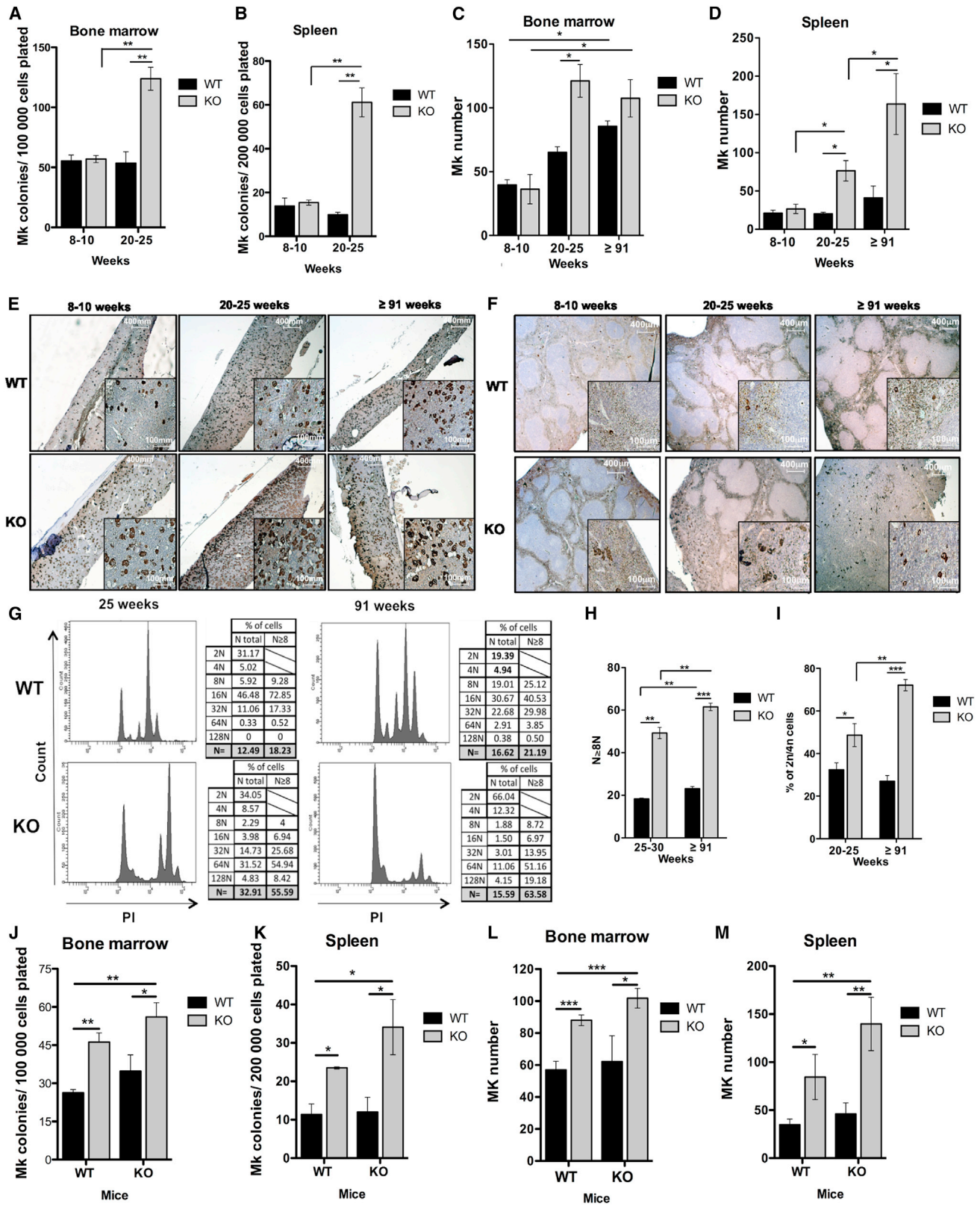

(legend on next page)

HSC pool (Scandura et al., 2004; Yamazaki and Nakauchi, 2009), while DNA damage accumulates in HSCs during aging (Rossi et al., 2007). As we demonstrated above, p19^{INK4d} protects HSCs from apoptosis during genotoxic stress. Loss of p19^{INK4d} could then alter the HSC pool during aging in both an intrinsic and extrinsic manner. Therefore, the number of LSK and SLAM cells was studied in aged animals (Figure 7A). No difference was observed in LSK cells during aging (Figure 7B). In agreement with previously published work (Beerman et al., 2010), we observed a 3-fold increase in SLAM cell numbers in WT mice more than 48 weeks old compared with 8- to 10-week-old mice, while only a slight increase was observed in the SLAM population of *p19$^{INK4d-/-}$* mice (Figure 7C). No difference in the total clonogenic potential between WT and *p19$^{INK4d-/-}$* SLAM cells from mice that were more than 48 weeks old was detected by in vitro assay on OP9/OP9Δ1 cell lines (Figure 7D).

The proportion of HSCs with myeloid potential increases with age, and this occurs at the expense of lymphoid potential (Beerman et al., 2010). Investigation of the myeloid versus lymphoid potential during aging (Figure 7E) confirmed an increase in HSC number in WT mice (2.2-fold), but not in *p19$^{INK4d-/-}$* mice (Figure 7F). In 8- to 10-week-old WT and *p19$^{INK4d-/-}$* mice, the lymphoid SP subpopulation was increased compared with its myeloid counterpart (Figures 7G and 7H). In WT mice, the proportion of myeloid SP increased 3.6-fold in old mice compared with young mice, and it exceeded the lymphoid SP fraction by 1.15-fold (Figures 7G and 7H). Moreover, *p19^{INK4d}* expression increased during aging in WT mice (Figure 7I). In contrast, the myeloid SP population in *p19$^{INK4d-/-}$* mice was only slightly amplified during aging, and no inversion in the ratio of lymphoid and myeloid SP was detected (Figures 7G and 7H).

To determine whether the age-related decrease of HSCs in *p19$^{INK4d-/-}$* mice is due to intrinsic and/or extrinsic effects of p19^{INK4d}, the numbers of LSK and SLAM from 8 month-old chimeric mice were analyzed (Figures 7J and 7L). As expected, the *p19$^{INK4d-/-}$* recipient mice that were reconstituted with *p19$^{INK4d-/-}$* cells (KO/KO) exhibited a 5.5- and 3.5-fold decrease in LSK (Figure 7K) and SLAM cell numbers (Figure 7M), respectively, compared with WT mice transplanted with WT cells (WT/WT). Surprisingly, when *p19$^{INK4d-/-}$* recipient mice were transplanted with WT cells (WT/KO), we observed respective decreases of 3.5- and 5.7-fold in LSK and SLAM cell numbers compared with WT/WT. Furthermore, when WT mice were transplanted with *p19$^{INK4d-/-}$* cells (KO/WT), a nonsignificant increase in LSK and SLAM numbers was observed compared with WT/WT. This suggests that there is increased turnover of *p19$^{INK4d-/-}$* cells in a WT environment.

These results clearly show that the absence of age-associated HSC amplification in a *p19$^{INK4d-/-}$* background is due exclusively to environmental effects that are caused by the loss of p19^{INK4d}.

Finally, we analyzed DNA-damage during aging. We observed an increase in ROS accumulation in *p19$^{INK4d-/-}$* LSK and SLAM cells (Figure 7N) that was associated with a slight increase in P-H2AX accumulation in *p19$^{INK4d-/-}$* LSK cells (Figures 7O and 7P). However, no increase in apoptosis was detected in *p19$^{INK4d-/-}$* LSK and SLAM cells (Figure 7Q). These results therefore indicate that p19^{INK4d} plays a crucial extrinsic role in the accumulation of HSCs with myeloid potential.

DISCUSSION

We report here that the p19^{INK4d} CDKI plays at least two important roles in regulation of the HSC pool. One of these is cell autonomous and manifests itself under conditions of stress. The second role relates to the microenvironment and underscores the role of p19^{INK4d} in mediating age-related effects on the HSC pool.

Figure 5. Absence of p19^{INK4d} Leads to a Progressive Age-Dependent Increase in the Number of MKs in BM and Spleen of Mice

(A and B) Number of MK-Ps derived from total BM cells (A) and total spleen cells (B) of 8- to 10-week-old (n = 3) and 20- to 25-week-old (n = 4) mice cultured in fibrin clots. Experiments were performed in triplicate for each biological replicate.

(C–F) Counts of MKs identified by vWF staining in BM (C) and spleen (D) of 8- to 10-week-old (n = 3), 20- to 25-week-old (n = 4) and in >91-week-old (n = 6) mice. The number of MKs was determined on equal areas of three independent image frames for each mouse. Representative pictures are shown for BM (E) and spleen (F).

(G) Cell cycle was measured by PI staining (middle panel) within the MK (CD41^{+}) population (left panel). Total and ≥8N MK ploidy level (right panel) was calculated for 20- to 25-week-old and >91-week-old mice.

(H) Mean ploidy level calculated for ≥8N MK.

(I) Percentage of 2N/4N MK cells in BM of 20- to 25-week-old and >91-week-old mice. Data represent mean ± SEM (n = 4) for 20- to 25-week-old and (n = 3) for >91-week-old mice.

(J and K) Number of MK-P derived from total BM cells (J) and total spleen cells (K) in 8-month-old transplanted WT and KO mice cultured in fibrin clots. Experiments were performed in triplicate for each biological replicate.

(L and M) Counts of MKs identified by vWF staining in BM (L) and spleen (M) in 8-month-old transplanted WT and KO mice (n = 5). The MK number was determined on equal areas of three independent image frames for each mouse.

KO, *p19$^{INK4d-/-}$*. Data represent mean ± SEM. *p < 0.05, **p < 0.01, ***p < 0.001, unpaired t test. See also Figure S3.

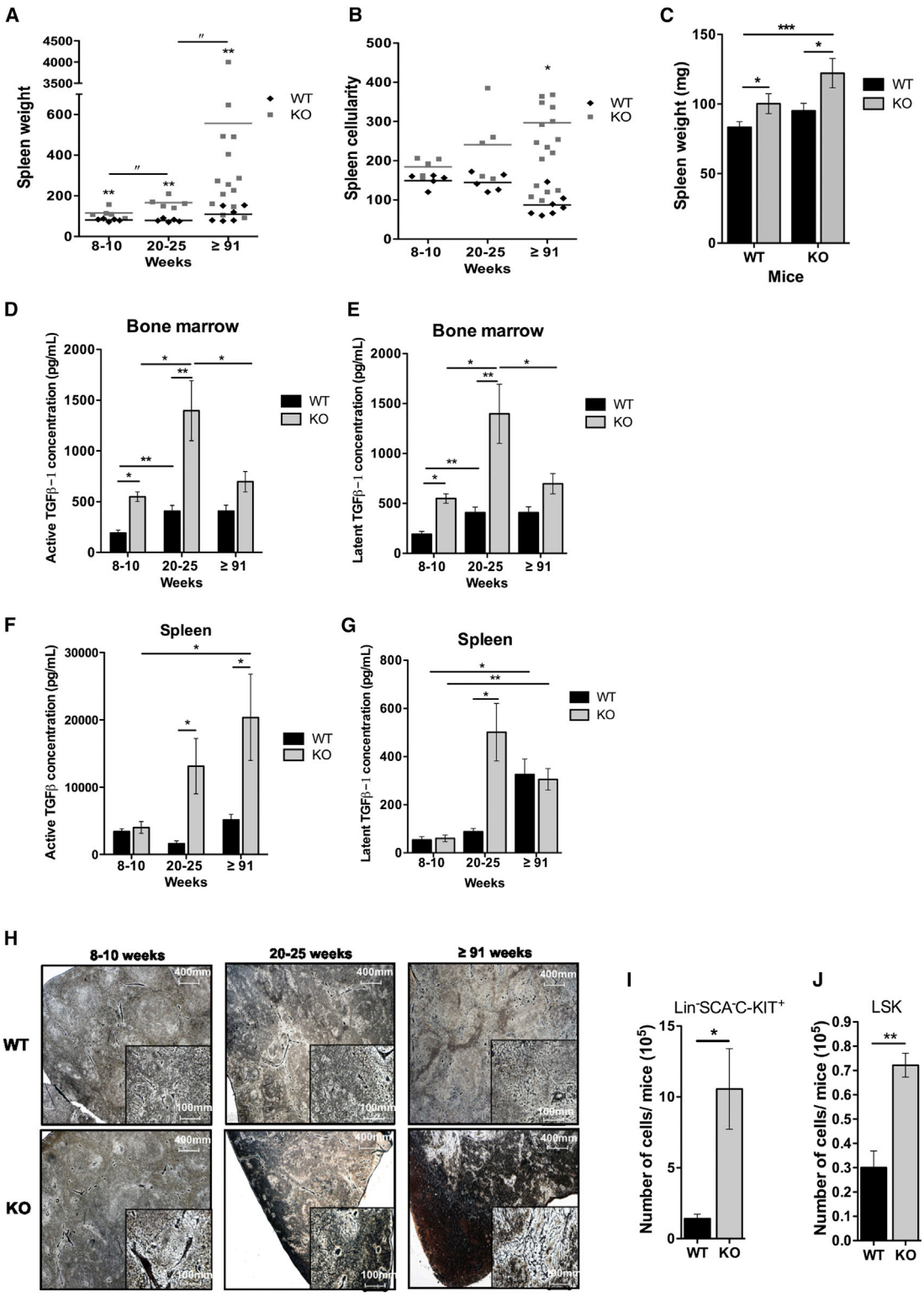

Figure 6. Megakaryopoiesis and Environment Defects in the Absence of p19INK4d Lead to the Development of Fibrosis

(A and B) Spleen weight (A) and cellularity (B) of 8- to 10-week-old (n = 5), 20- to 25-week-old (n = 5) and >91-week-old (n = 6 for WT and n = 14 for KO) mice. Each dot represents data from a single mouse. The * shows the differences between WT and KO mice, and the ″ shows differences between 8- to 10-week-old and 20- to 25-week-old mice or between 8- to 10-week-old and >91-week-old KO mice.

(legend continued on next page)

Cell Autonomous Role of p19INK4d in HSCs under Basal and Stress Conditions

The first preliminary evidence for a role of p19INK4d in the regulation of HSC quiescence came from the observation that *Thpo*$^{-/-}$ mice exhibited a decreased number of dormant HSCs that was associated with decreased p19INK4d and p57CDKN1c expression (Qian et al., 2007). Our studies revealed that *p19*$^{INK4d-/-}$ mice displayed a slight decrease in the absolute number of HSCs, which decreased further with age. This was particularly the case for HSCs with myeloid potential. As previously described in other cellular models, our in vivo study of HSC proliferation demonstrates increased apoptosis in the absence of p19INK4d. An association between loss of p19INK4d and re-entry into the cell cycle followed by apoptosis has been reported for neurons (Zindy et al., 1999) and terminally differentiated hair cells (Chen et al., 2003). However, in our study, apoptosis in the HSC compartment was measured after in vivo administration of BrdU, which may inherently induce stress. To further investigate the role of p19INK4d in this context, we induced three types of stress. First, we used 5-FU, which induces both replicative and genotoxic stresses in quiescent HSCs. Second, we used menadione, which is a genotoxic agent that induces DNA damage through elevated ROS levels. Third, we used HU, which induces replicative rather than genotoxic stress. Our results clearly demonstrate that 5-FU injection leads to enhanced mortality of *p19*$^{INK4d-/-}$ mice that is associated with a marked increase in apoptosis following the exit of HSCs from quiescence. The same outcome was observed when *p19*$^{INK4d-/-}$ cells were transplanted into WT recipients, thereby confirming a cell-autonomous role of p19INK4d. In light of the massive apoptosis in the S/G2-M phases that occurs following menadione treatment, and the absence of apoptosis after HU treatment, these results indicate that p19INK4d is required to protect HSCs from apoptosis under conditions of genotoxic stress, but not the replicative stress induced by HU. Additional experiments are necessary, however, to clearly define the roles of p19INK4d after induction of these two types of stress. Previous studies have demonstrated that p19INK4d contributes to DNA repair, apoptotic, and checkpoint mechanisms in order to maintain integrity of the genome under conditions of genotoxic stress, in a manner that is independent of CDK4/6 inhibition (Ogara et al., 2013; Scassa et al., 2007). Our data suggest that HSC cell cycle entry is enhanced by p19INK4d loss as a result of CDK4/6-dependent functions but that CDK4/6-independent p19INK4d functions contribute to reduced HSC numbers following increased apoptosis in the S/G2-M phases of the cell cycle. This mechanism may operate preferentially during genotoxic stress because *p19*$^{INK4d-/-}$ HSCs have normal reconstitutive capacities in BM transplant experiments.

Extrinsic Role of p19INK4d in the BM Niche: Development of Myelofibrosis in the Absence of p19INK4d

The effect of p19INK4d on the HSC compartment is, however, not purely cell autonomous. A significant decrease in the number of HSCs was observed in *p19*$^{INK4d-/-}$ mice even in the absence of stress induction, but *p19*$^{INK4d-/-}$ BM Lin$^-$ cells display a competitive advantage compared with controls after transplantation into WT recipients. This strongly suggests that the HSC microenvironment is also defective in *p19*$^{INK4d-/-}$ mice.

There is evidence that MKs play an important role in HSC regulation. We previously reported that p19INK4d regulates MK ploidy (Gilles et al., 2008). By further investigating the MK lineage, we also detected an increase in MK-P and mature MK numbers in *p19*$^{INK4d-/-}$ mice with an increased proportion of proliferative 2N/4N MKs during aging. Moreover, we demonstrated that the number of MKs increased with age in the BM of WT mice, but did not change in the spleen. In contrast, MK numbers increased in the spleens of *p19*$^{INK4d-/-}$ mice after reaching a plateau in the BM, leading to splenomegaly and fibrosis in both the BM and spleen. This phenotype was accompanied by increased levels of total and bioactive TGF-β1 in the extracellular fluids of the BM and spleen. MK and platelet α granules are the principal storage sites for TGF-β1, and myelofibrosis occurring in myeloid disorders is often associated with a marked MK hyperplasia and increased TGF-β1 release into the BM microenvironment. Interestingly, there was a striking similarity between the phenotype of aged *p19*$^{INK4d-/-}$ mice and human primary myelofibrosis (PMF), which is characterized by splenomegaly and myelofibrosis with

(C) Spleen weights of 8-month-old transplanted mice (n = 5). Data represent mean ± SEM.
(D and E) Dosage by ELISA of total TGF-β1 in fluids extracted from BM (D) and spleen (E) of 8- to 10-week-old (n = 5), 20- to 25-week-old (n = 3) and >91-week-old (n = 3 for WT and n = 8 for KO) mice.
(F and G) Dosage of latent TGF-β1 in fluids extracted from BM (F) and spleen (G) of 8- to 10-week-old (n = 5), 20- to 25-week-old (n = 3) and >91-week-old (n = 3 for WT and n = 8 for KO) mice.
(H) Data represent mean ± SEM. Representative images of 8- to 10-week-old, 20- to 25-week-old, and >91-week-old mice spleens stained for reticulin, highlighting the fibrotic status of the tissue.
(I and J) Number of Lin$^-$SCA1$^-$C-KIT$^+$ (I) and LSK (J) cells in peripheral blood of >91-week-old mice. Data represent mean ± SEM (n = 4). KO: *p19*$^{INK4d-/-}$. Data represent mean ± SEM. *p < 0.05, **p < 0.01, ***p < 0.001, unpaired t test. See also Figure S4.

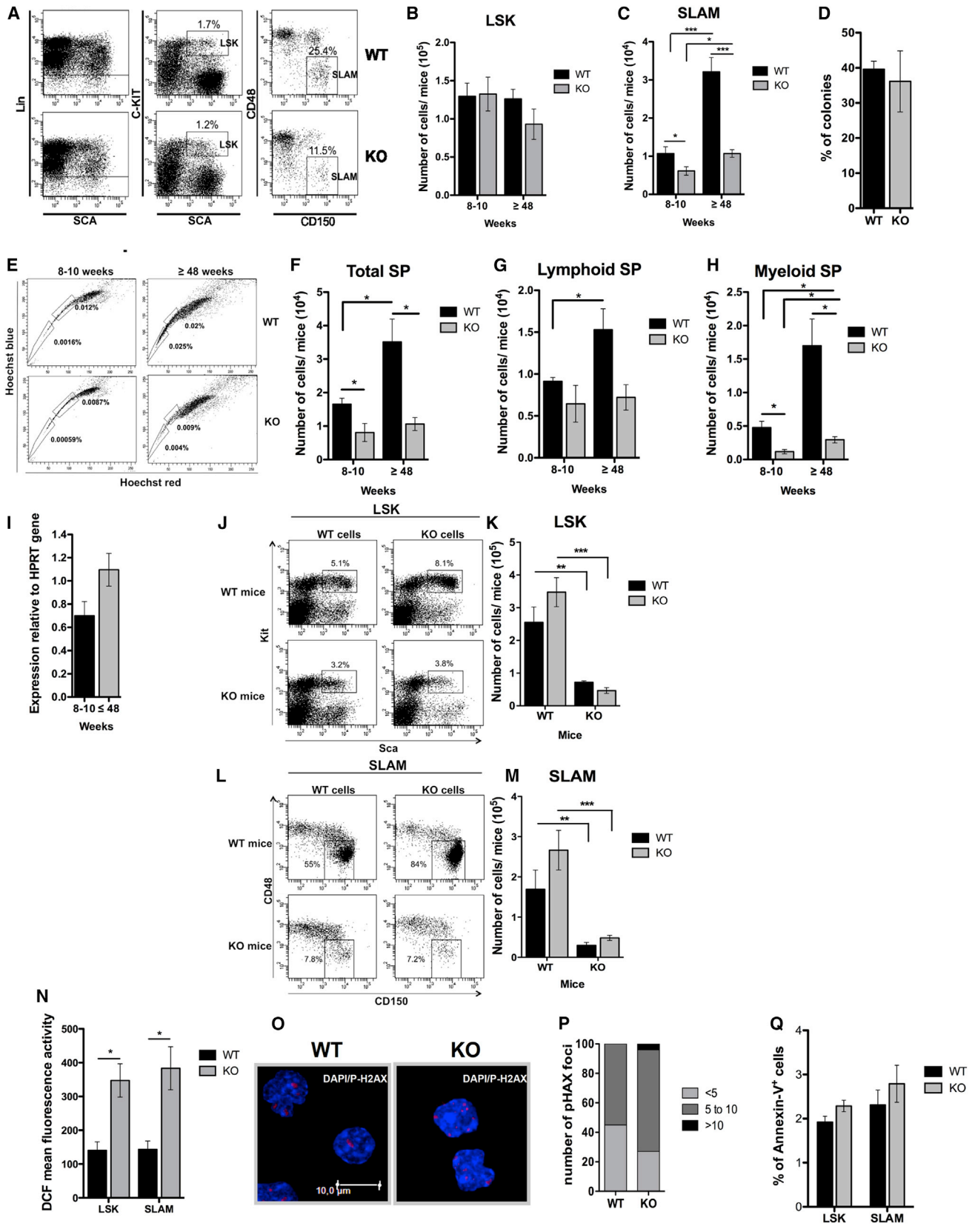

(legend on next page)

osteomyelosclerosis. Similar to PMF, an increase in circulating HSPs was observed in *p19$^{INK4d-/-}$* animals. Human PMF has been associated with acquired mutations in signaling molecules such as JAK2, MPL, and CALR, all of which lead to JAK/STAT pathway activation (Klampfl et al., 2013; Nangalia et al., 2013). How these mutations contribute to the myelofibrosis development has not been completely elucidated. There is, however, strong evidence that the myelofibrosis is a response to the in situ release of myeloid-derived factors such as TGF-β1, platelet-derived growth factor, vascular endothelial growth factor, and other proinflammatory cytokines. It is likely that MKs are the key cells in the development of myelofibrosis because increased proliferation of dysplastic MKs is a hallmark of PMF, with the onset of fibrosis occurring around dysplastic MK clusters. This is further supported by different mouse models of myelofibrosis, such as JAK2^{V617F} (Lacout et al., 2006), MPL$^{W515L/A}$ (Pikman et al., 2006), TPO^{high} (Villeval et al., 1997), or GATA1^{low} (Vannucchi et al., 2002) systems. GATA1 is one of the major cofactors of the transcription factor RUNX1 in MKs (Tijssen et al., 2011). We have previously shown that p19^{INK4d} is directly regulated by RUNX1 in MKs (Gilles et al., 2008), suggesting that p19^{INK4d} expression could be altered in MK progenitors of GATA1^{low} mice.

We provide evidence that, as in human PMF, the fibrosis observed in *p19$^{INK4d-/-}$* mice is related to abnormal hematopoiesis. Indeed, splenomegaly and increased MK numbers were detected in recipient WT mice transplanted with *p19$^{INK4d-/-}$* cells, but not in *p19$^{INK4d-/-}$* recipient mice transplanted with WT cells. This suggests that the development of fibrosis is dependent on *p19$^{INK4-/-}$* hematopoietic cells. However, our in vitro experiments indicate that *p19$^{INK4d-/-}$* stroma also has a decreased capacity to sustain hematopoiesis. This is reminiscent of the in vitro stromal defects observed in myeloid malignancies, including PMF. Whether this defect is related to stromal epigenetic modifications due to abnormal myeloid proliferation or to a primary intrinsic defect in the BM environment, however, remains controversial. Regardless, the phenotype of *p19$^{INK4d-/-}$* mice underscores the role of MKs not only in the development of myelofibrosis, but also in the regulation of the hematopoietic niche.

During their life span, HSCs undergo changes in the proportions of different subpopulations. HSC aging is characterized by an imbalance in the myelo-lymphopoiesis ratio, leading to amplification of myeloid-biased HSCs, progressive loss of lymphoid-biased HSCs (Challen et al., 2010), and accumulation of DNA damage (Rossi et al., 2007). The higher self-renewal capacity of myeloid HSCs that is associated with the accumulation of DNA damage with age likely contributes to the increased frequency of myeloid malignancies observed in elderly individuals. We demonstrate here that p19^{INK4d} loss enhances accumulation of DNA-DSBs during aging, although the major effect of p19^{INK4d} on the amplification of myeloid-biased HSCs during aging is clearly related to the microenvironment. Further studies to determine the precise mechanism by which this occurs are required. One potential explanation could be an age-associated increase in TGF-β1 levels produced by MKs. High levels of TGF-β1 may contribute to decreased numbers of HSCs (Scandura et al., 2004) observed in *p19$^{INK4d-/-}$* animals during aging. On the other hand and in contrast to our observations in the absence of p19^{INK4d}, it has been shown that TGF-β1 may expand myeloid-biased HSCs and inhibit the lymphoid-biased HSC population that occurs with aging (Challen et al., 2010). However, we demonstrate that increasing p19^{INK4d} expression in HSCs during aging is clearly associated with an increase in myeloid-biased HSCs, indicating that TGF-β1 may regulate myeloid-biased HSCs through p19^{INK4d}.

In conclusion, we report a mechanism by which fibrosis can be induced by loss of a protein, p19^{INK4d}, that plays a crucial role in regulating the MK cell cycle. Whether

Figure 7. Defect in HSC Amplification during Aging Is Primarily due to Environmental Effects Induced by p19^{INK4d} Loss

(A–C) Immunophenotype (A) and number of LSK (B) and SLAM (C) cells in 8- to 10-week-old (n = 8) and >48-week-old mice (n = 4).

(D) Assessment of biological functions in HSCs of >48-week-old mice (n = 3). For each condition, 144 SLAM cells were plated at one cell/well on OP9/OP9Δ1 stromal cells.

(E–H) Immunophenotype (E) and number of total SP (F), lymphoid SP (G), and myeloid SP (H) cells in 8- to 10-week-old (n = 4) and >48-week-old (n = 3) WT and KO mice.

(I) *p19^{INK4d}* transcript level in WT SLAM cells during aging. Data are normalized to *HPRT* levels and represent mean ± SEM of triplicate experiments.

(J–M) Immunophenotype (J and L) and number of LSK (K) and SLAM (M) cells in 8-month-old transplanted mice, KO mice transplanted with WT cells (n = 3), WT mice transplanted with WT cells (n = 4), WT mice transplanted with KO cells (n = 5), and KO mice transplanted with KO cells (n = 5).

(N) DCF mean fluorescence in LSK and SLAM cells in >48-week-old mice (n = 4).

(O and P) P-H2AX staining in LSK cells in 48-week-old mice. Representative pictures (O) are shown. Nuclei are stained with DAPI (blue), and DNA-DSBs are stained by an anti-P-H2AX antibody (red). (P) The number of P-H2AX foci per 100 LSK cells.

(Q) Apoptosis assessment in LSK and SLAM populations in >48-week-old mice (n = 4).

KO: *p19$^{INK4d-/-}$*. Data represent mean ± SEM. *p < 0.05, **p < 0.01, ***p < 0.001, unpaired t test.

p19^{INK4d} could be an indirect target of signaling molecules that have been genetically altered in human PMF remains to be investigated. The results presented here also underscore the protective role of p19^{INK4d} during genotoxic stress and demonstrate that p19^{INK4d} plays an important role in hematopoiesis, including the changes that occur during aging. This study hence opens avenues of research for the delineation of this gene's precise function in HSCs and their microenvironmental niche.

EXPERIMENTAL PROCEDURES

Mice

Heterozygous *p19$^{INK4d(+/-)}$* (C57BL/6 × Sv129j) mice (Zindy et al., 2000) were obtained from Martine Roussel. WT and *p19$^{INK4d-/-}$* mice were obtained by intercrossing heterozygous mice. All animal experiments were approved by the local Ethical Committee of University Paris-Sud no. 26 (authorized project no. 2012-060).

Flow Cytometry

LSK, progenitors, or mature cells were analyzed on FACS LSR II or FACS CANTO II (BD) and sorted on MoFlo or Influx flow cytometers (BD). SP staining and MK ploidy analyses were performed as previously described (Goodell et al., 1996; Gilles et al., 2008). HSC cell cycle analysis was performed with either Ki-67/Hoechst 33342 or BrdU/Hoechst 33342 costaining.

Reconstitution Assays

To study the role of the environment in hematopoietic reconstitution, *p19$^{INK4d-/-}$* and WT mice were lethally irradiated (11 Gy). After 24 hr, the mice were reconstituted with 2 × 10^6 WT or *p19$^{INK4d-/-}$* total BM cells. The reconstitution potential was evaluated as survival rate and cell cycle and apoptosis assays were performed. To evaluate the reconstitution advantage of *p19$^{INK4d-/-}$* or WT cells, competitive transplantation was performed with 5 × 10^4 WT-GFP: 5 × 10^4 *p19$^{INK4d-/-}$* CHERRY cells. Blood was sampled once per month to follow hematopoietic reconstitution. Mice were euthanized 3.5 months after transplantation. BM cells were collected, and different populations were analyzed by flow cytometry to determine the proportion of GFP$^+$ and CHERRY$^+$ cells.

In primary and secondary transplantation assays, 5 × 10^6 cells from whole spleen of myelofibrotic mice were injected intraorbitally into lethally irradiated recipient WT mice. For secondary transplantation assays, spleen cells were collected 2 months after transplantation. Half of the spleen and one femur were retained for each mouse in order to perform immunohistochemistry.

Treatment for Myelosuppression by Administration of 5-FU

Mice were injected intraperitoneally with 5-FU (Fluorouracil, Dakota Pharm) at 150 mg/kg body weight for survival rates of mice and at 250 or 50 mg/kg body weight for cell cycle analysis in nontransplanted or transplanted mice, respectively.

Stress Induction with HU Treatment

Mice were treated with HU (100 mg/kg/day) by intraperitoneal injection for three consecutive days, and cell cycle analysis and apoptosis assays were subsequently performed.

Oxidative Stress Induction

Lin$^-$ cells were incubated with or without menadione (10 mM) for 1 hr, and LSKs were then stained to measure ROS levels. ROS production was monitored by flow cytometry using 2′,7′ dichlorodihydrofluorescin diacetate ($DCFH_2$-DA).

Statistical Analysis

Results were evaluated by performing unpaired t tests using GraphPad Prism version 5.0 software (GraphPad Software). Results are presented as means ± SEM. *$p < 0.05$ was determined significant, and **$p < 0.01$ or ***$p < 0.001$ were considered highly significant; "n =" stands for individual mice in all experiments.

SUPPLEMENTAL INFORMATION

Supplemental Information includes Supplemental Experimental Procedures, four figures, and one table and can be found with this article online at http://dx.doi.org/10.1016/j.stemcr.2014.10.005.

ACKNOWLEDGMENTS

This work was supported by French grants from the Agence Nationale de la Recherche (H.R.), the Ligue Nationale contre le Cancer (équipe labellisée 2009 [W.V.] and 2013 [H.R.]). M.H. was supported by the ARC. We thank P. Rameau and Y. Lecluse for flow cell analysis and sorting and O. Bawa for immunohistochemistry (IRCIV, Institut Gustave Roussy). We are grateful to Professor R. Skoda (University Hospital of Basel) and Professor J.D. Crispino (Northwestern University) for helpful discussions, and Dr. B.J. Thompson (Northwestern University) and Dr. K. Rice (Hospital St. Louis) for English editing.

Received: April 24, 2014
Revised: October 15, 2014
Accepted: October 15, 2014
Published: November 20, 2014

REFERENCES

Adachi, M., Roussel, M.F., Havenith, K., and Sherr, C.J. (1997). Features of macrophage differentiation induced by p19INK4d, a specific inhibitor of cyclin D-dependent kinases. Blood *90*, 126–137.

Attema, J.L., Pronk, C.J., Norddahl, G.L., Nygren, J.M., and Bryder, D. (2009). Hematopoietic stem cell ageing is uncoupled from p16 INK4A-mediated senescence. Oncogene *28*, 2238–2243.

Beerman, I., Bhattacharya, D., Zandi, S., Sigvardsson, M., Weissman, I.L., Bryder, D., and Rossi, D.J. (2010). Functionally distinct hematopoietic stem cells modulate hematopoietic lineage potential during aging by a mechanism of clonal expansion. Proc. Natl. Acad. Sci. USA *107*, 5465–5470.

Ceruti, J.M., Scassa, M.E., Marazita, M.C., Carcagno, A.C., Sirkin, P.F., and Cánepa, E.T. (2009). Transcriptional upregulation of p19INK4d upon diverse genotoxic stress is critical for optimal DNA damage response. Int. J. Biochem. Cell Biol. *41*, 1344–1353.

Challen, G.A., Boles, N.C., Chambers, S.M., and Goodell, M.A. (2010). Distinct hematopoietic stem cell subtypes are differentially regulated by TGF-beta1. Cell Stem Cell *6*, 265–278.

Chen, P., Zindy, F., Abdala, C., Liu, F., Li, X., Roussel, M.F., and Segil, N. (2003). Progressive hearing loss in mice lacking the cyclin-dependent kinase inhibitor Ink4d. Nat. Cell Biol. *5*, 422–426.

Cheng, T., Rodrigues, N., Dombkowski, D., Stier, S., and Scadden, D.T. (2000a). Stem cell repopulation efficiency but not pool size is governed by p27(kip1). Nat. Med. *6*, 1235–1240.

Gilles, L., Guièze, R., Bluteau, D., Cordette-Lagarde, V., Lacout, C., Favier, R., Larbret, F., Debili, N., Vainchenker, W., and Raslova, H. (2008). P19INK4D links endomitotic arrest and megakaryocyte maturation and is regulated by AML-1. Blood *111*, 4081–4091.

Goodell, M.A., Brose, K., Paradis, G., Conner, A.S., and Mulligan, R.C. (1996). Isolation and functional properties of murine hematopoietic stem cells that are replicating in vivo. J. Exp. Med. *183*, 1797–1806.

Hidalgo, I., Herrera-Merchan, A., Ligos, J.M., Carramolino, L., Nuñez, J., Martinez, F., Dominguez, O., Torres, M., and Gonzalez, S. (2012). Ezh1 is required for hematopoietic stem cell maintenance and prevents senescence-like cell cycle arrest. Cell Stem Cell *11*, 649–662.

Janzen, V., Forkert, R., Fleming, H.E., Saito, Y., Waring, M.T., Dombkowski, D.M., Cheng, T., DePinho, R.A., Sharpless, N.E., and Scadden, D.T. (2006). Stem-cell ageing modified by the cyclin-dependent kinase inhibitor p16INK4a. Nature *443*, 421–426.

Klampfl, T., Gisslinger, H., Harutyunyan, A.S., Nivarthi, H., Rumi, E., Milosevic, J.D., Them, N.C., Berg, T., Gisslinger, B., Pietra, D., et al. (2013). Somatic mutations of calreticulin in myeloproliferative neoplasms. N. Engl. J. Med. *369*, 2379–2390.

Lacout, C., Pisani, D.F., Tulliez, M., Gachelin, F.M., Vainchenker, W., and Villeval, J.L. (2006). JAK2V617F expression in murine hematopoietic cells leads to MPD mimicking human PV with secondary myelofibrosis. Blood *108*, 1652–1660.

Mascarenhas, M.I., Parker, A., Dzierzak, E., and Ottersbach, K. (2009). Identification of novel regulators of hematopoietic stem cell development through refinement of stem cell localization and expression profiling. Blood *114*, 4645–4653.

Matsumoto, A., Takeishi, S., Kanie, T., Susaki, E., Onoyama, I., Tateishi, Y., Nakayama, K., and Nakayama, K.I. (2011). p57 is required for quiescence and maintenance of adult hematopoietic stem cells. Cell Stem Cell *9*, 262–271.

Nangalia, J., Massie, C.E., Baxter, E.J., Nice, F.L., Gundem, G., Wedge, D.C., Avezov, E., Li, J., Kollmann, K., Kent, D.G., et al. (2013). Somatic CALR mutations in myeloproliferative neoplasms with nonmutated JAK2. N. Engl. J. Med. *369*, 2391–2405.

Ogara, M.F., Sirkin, P.F., Carcagno, A.L., Marazita, M.C., Sonzogni, S.V., Ceruti, J.M., and Cánepa, E.T. (2013). Chromatin relaxation-mediated induction of p19INK4d increases the ability of cells to repair damaged DNA. PLoS ONE *8*, e61143.

Passegué, E., Wagers, A.J., Giuriato, S., Anderson, W.C., and Weissman, I.L. (2005). Global analysis of proliferation and cell cycle gene expression in the regulation of hematopoietic stem and progenitor cell fates. J. Exp. Med. *202*, 1599–1611.

Pikman, Y., Lee, B.H., Mercher, T., McDowell, E., Ebert, B.L., Gozo, M., Cuker, A., Wernig, G., Moore, S., Galinsky, I., et al. (2006). MPLW515L is a novel somatic activating mutation in myelofibrosis with myeloid metaplasia. PLoS Med. *3*, e270.

Qian, H., Buza-Vidas, N., Hyland, C.D., Jensen, C.T., Antonchuk, J., Månsson, R., Thoren, L.A., Ekblom, M., Alexander, W.S., and Jacobsen, S.E. (2007). Critical role of thrombopoietin in maintaining adult quiescent hematopoietic stem cells. Cell Stem Cell *1*, 671–684.

Rossi, D.J., Bryder, D., Seita, J., Nussenzweig, A., Hoeijmakers, J., and Weissman, I.L. (2007). Deficiencies in DNA damage repair limit the function of haematopoietic stem cells with age. Nature *447*, 725–729.

Scandura, J.M., Boccuni, P., Massagué, J., and Nimer, S.D. (2004). Transforming growth factor beta-induced cell cycle arrest of human hematopoietic cells requires p57KIP2 up-regulation. Proc. Natl. Acad. Sci. USA *101*, 15231–15236.

Scassa, M.E., Marazita, M.C., Ceruti, J.M., Carcagno, A.L., Sirkin, P.F., González-Cid, M., Pignataro, O.P., and Cánepa, E.T. (2007). Cell cycle inhibitor, p19INK4d, promotes cell survival and decreases chromosomal aberrations after genotoxic insult due to enhanced DNA repair. DNA Repair (Amst.) *6*, 626–638.

Tijssen, M.R., Cvejic, A., Joshi, A., Hannah, R.L., Ferreira, R., Forrai, A., Bellissimo, D.C., Oram, S.H., Smethurst, P.A., Wilson, N.K., et al. (2011). Genome-wide analysis of simultaneous GATA1/2, RUNX1, FLI1, and SCL binding in megakaryocytes identifies hematopoietic regulators. Dev. Cell *20*, 597–609.

van Os, R., Kamminga, L.M., Ausema, A., Bystrykh, L.V., Draijer, D.P., van Pelt, K., Dontje, B., and de Haan, G. (2007). A Limited role for p21Cip1/Waf1 in maintaining normal hematopoietic stem cell functioning. Stem Cells *25*, 836–843.

Vannucchi, A.M., Bianchi, L., Cellai, C., Paoletti, F., Rana, R.A., Lorenzini, R., Migliaccio, G., and Migliaccio, A.R. (2002). Development of myelofibrosis in mice genetically impaired for GATA-1 expression (GATA-1(low) mice). Blood *100*, 1123–1132.

Villeval, J.L., Cohen-Solal, K., Tulliez, M., Giraudier, S., Guichard, J., Burstein, S.A., Cramer, E.M., Vainchenker, W., and Wendling, F. (1997). High thrombopoietin production by hematopoietic cells induces a fatal myeloproliferative syndrome in mice. Blood *90*, 4369–4383.

Yamazaki, S., and Nakauchi, H. (2009). Insights into signaling and function of hematopoietic stem cells at the single-cell level. Curr. Opin. Hematol. *16*, 255–258.

Yoshihara, H., Arai, F., Hosokawa, K., Hagiwara, T., Takubo, K., Nakamura, Y., Gomei, Y., Iwasaki, H., Matsuoka, S., Miyamoto, K., et al. (2007). Thrombopoietin/MPL signaling regulates hematopoietic stem cell quiescence and interaction with the osteoblastic niche. Cell Stem Cell *1*, 685–697.

Yuan, Y., Yu, H., Boyer, M.J., Song, X., Cao, S., Shen, H., and Cheng, T. (2006). Hematopoietic stem cells are not the direct target of spontaneous leukemic transformation in p18(INK4C)-null reconstituted mice. Cancer Res. *66*, 343–351.

Zindy, F., Cunningham, J.J., Sherr, C.J., Jogal, S., Smeyne, R.J., and Roussel, M.F. (1999). Postnatal neuronal proliferation in mice lacking Ink4d and Kip1 inhibitors of cyclin-dependent kinases. Proc. Natl. Acad. Sci. USA *96*, 13462–13467.

Zindy, F., van Deursen, J., Grosveld, G., Sherr, C.J., and Roussel, M.F. (2000). INK4d-deficient mice are fertile despite testicular atrophy. Mol. Cell. Biol. *20*, 372–378.

Zindy, F., den Besten, W., Chen, B., Rehg, J.E., Latres, E., Barbacid, M., Pollard, J.W., Sherr, C.J., Cohen, P.E., and Roussel, M.F. (2001). Control of spermatogenesis in mice by the cyclin D-dependent kinase inhibitors p18(Ink4c) and p19(Ink4d). Mol. Cell. Biol. *21*, 3244–3255.

Stem Cell Reports, Volume *3*

Supplemental Information

$p19^{INK4d}$ Controls Hematopoietic Stem Cells in a Cell-Autonomous Manner during Genotoxic Stress and through the Microenvironment during Aging

Morgane Hilpert, Céline Legrand, Dominique Bluteau, Natalie Balayn, Aline Betems, Olivier Bluteau, Jean-Luc Villeval, Fawzia Louache, Patrick Gonin, Najet Debili, Isabelle Plo, William Vainchenker, Laure Gilles, and Hana Raslova

Supplemental figures and legends

Figure S1

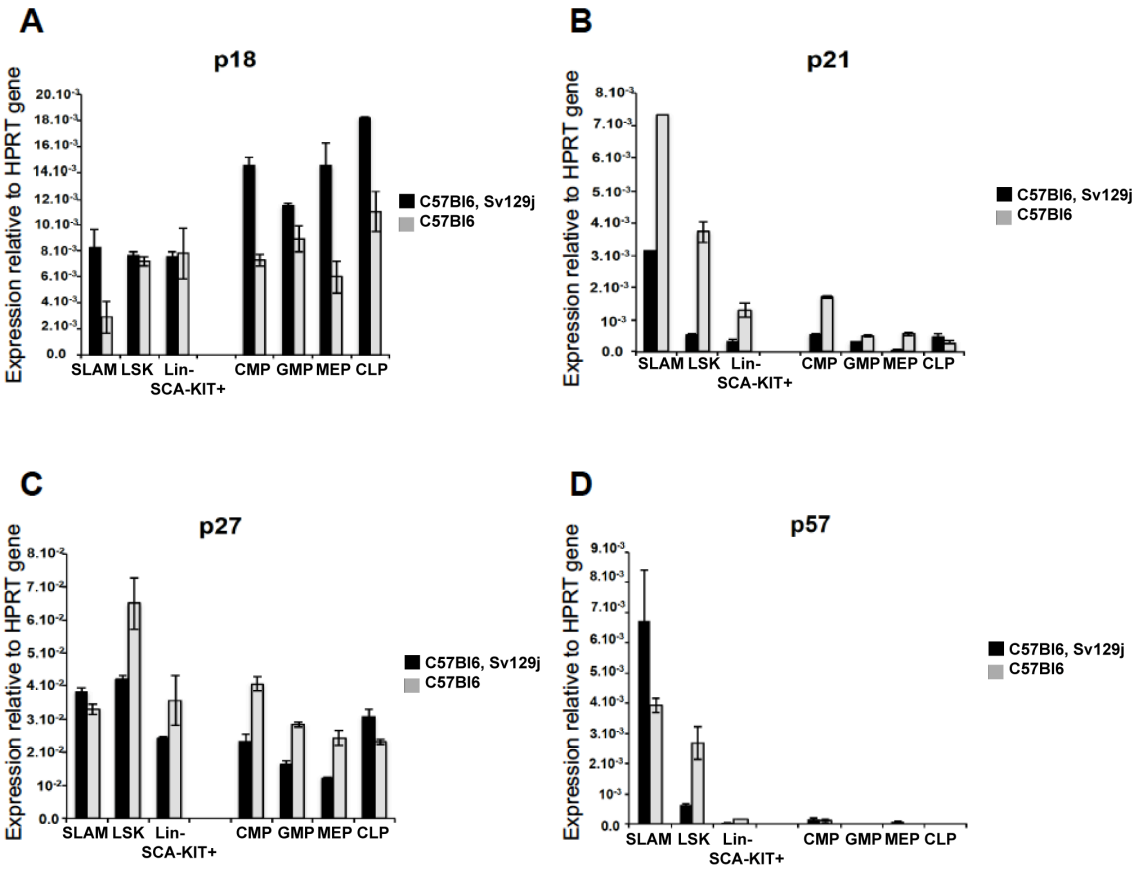

Figure S1, related to Figure 1. Expression of different CDKIs in C57Bl6 and C57Bl6/Sv129J mice.

(A-D) mRNA expression levels of *p18*^{Ink4c} **(A)**, *p21*^{CIP1} **(B)**, *p27*^{KIP1} **(C)** and *p57*^{KIP2} **(D)** measured by qRT-PCR in different progenitor cell populations of C57BL/6 and mixed C57BL/6-Sv129J mice. SLAM ($Lin^-SCA1^+C\text{-}KIT^+CD48^-CD150^+$), LSK ($Lin^-SCA1^+C\text{-}KIT^+$), myeloid progenitors ($Lin^-SCA1^-C\text{-}KIT^+$), CLP ($Lin^-SCA1^{low}C\text{-}KIT^{low}CD127^+THY\text{-}1^-$), CMP ($Lin^-SCA1^-C\text{-}KIT^+FC\gamma R^-CD34^+$), GMP ($Lin^-SCA1^-C\text{-}KITt^+FC\gamma R^+CD34^+$) and MEP ($Lin^-SCA1^-C\text{-}KIT^+FC\gamma R^-CD34^-$) populations were sorted by flow cytometry. Each population

represents a pool derived from 10 mice. Data are normalized to *HPRT* transcript levels and represent the mean ± SEM of biological triplicate experiments.

Figure S2

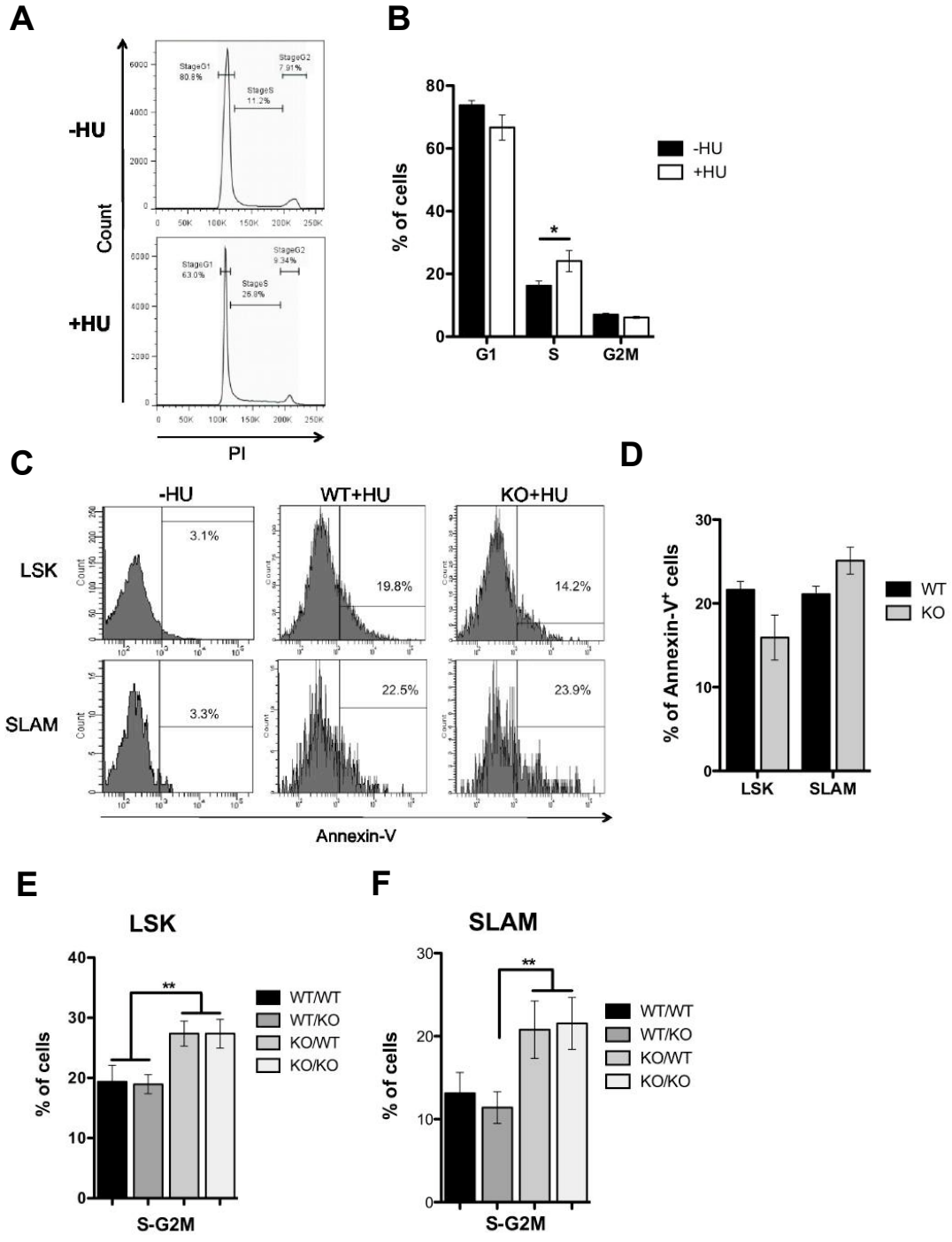

Figure S2, related to Figure 3. Cell cycle analysis during genotoxic and replicative stress.

(A, B) Cell cycle analysis by PI staining of Lin$^-$ cells in mice with or without HU treatment. Representative cell cycle histogram **(A)** and frequencies of cells in different phases of the cell

cycle **(B)**. Data represent mean ± SEM (n=7). **(C, D)** Immunophenotype **(C)** and apoptosis (annexin-V-positive cells) **(D)** in LSK and SLAM populations of WT and KO mice after HU treatment. **(E, F)** Cell cycle analysis by Ki-67/Hoechst co-staining two days after 5-FU injection. Frequencies of S-G2M phases in LSK **(E)** and SLAM **(F)** populations in 2 month-old transplanted WT and KO mice. Data represent mean ± SEM (n=6). *p<0.05, **p<0.01. WT: wild type, KO: $p19^{INK4d-/-}$, unpaired *t* test.

Figure S3

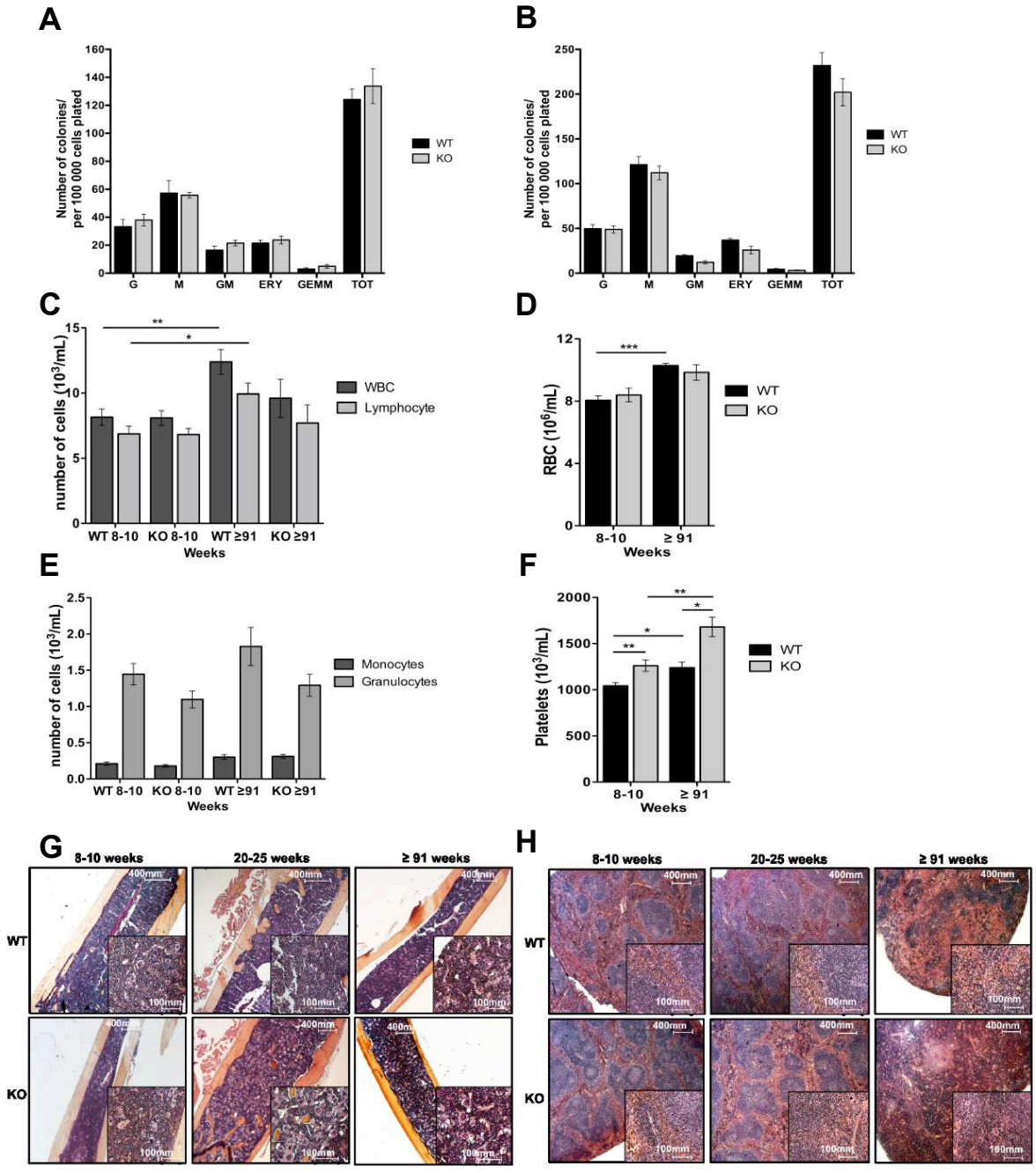

Figure S3, related to Figure 5. Assessment of myeloid progenitors and whole blood cell populations in WT and *p19*$^{INK4d-/-}$ mice during aging.

(A, B) Progenitor assays in methylcellulose cultures of BM cells from 8-10 week-old **(A)** and > 48 week-old **(B)** WT and KO mice. Experiments were performed in triplicate for each biological replicate. Error bars represent mean ± SEM, n=4. G= Granulocyte colony, M=

Monocytes/Macrophage colony, GM= Granulo-Macrophage colony, ERY= Erythroid colony, GEMM= Granulocyte, Erythroid, Megakaryocyte, Monocyte/Macrophage colony, TOT= total colony number. **(C-F)** Whole blood cell analysis in 8-10 (n=10) and > 91 (n=4) week-old WT and KO mice. Data represent mean ± SEM **(C)** White blood cell (WBC) and lymphocyte counts, **(D)** Red blood cell (RBC) counts, **(E)** Monocyte and granulocyte counts, **(F)** Platelet counts, **(G, H)** HES staining of BM **(G)** and spleen **(H)** from 8-10 (n=4), 20-25 (n=5) and > 91 (n=3 for WT and n=8 for KO) week-old WT and KO mice. Representative picture of BM and spleen of one mouse is shown.

WT: wild type, KO: $p19^{INK4d-/-}$,*p<0.05, **p<0.01, ***p<0.001, unpaired *t* test.

Figure S4

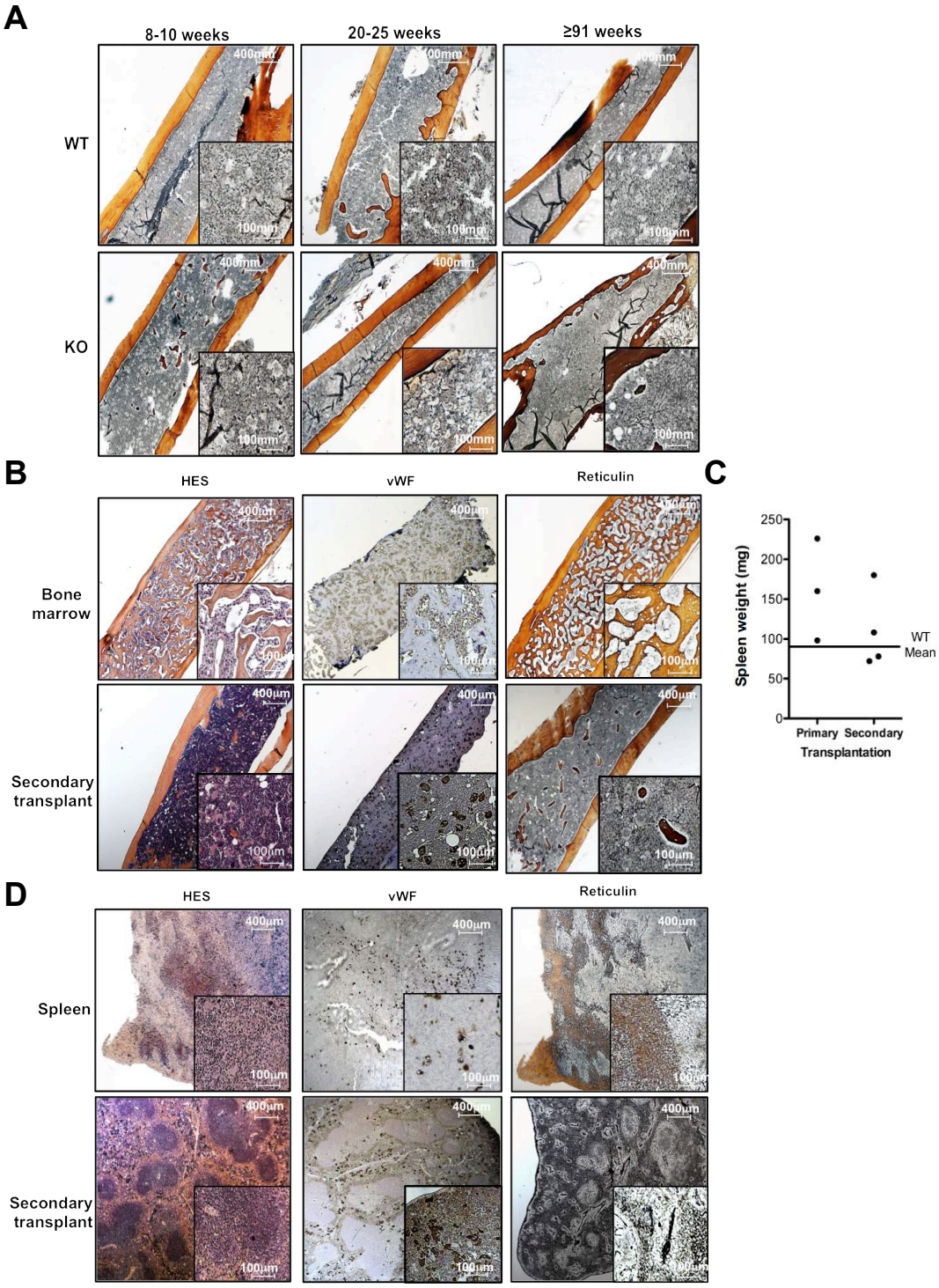

Figure S4, related to Figure 6. Progressive fibrosis development with age in the absence of p19^{INK4d}

(A) Reticulin staining of BM in 8-10, 20-25 and > 91 week-old mice. Representative picture of reticulin staining in BM of one mouse is shown, **(B-D)** Engraftment of a 4g fibrotic spleen in primary and secondary recipients. Representative pictures of HES, vWF and reticulin staining in BM **(B)** and spleen **(D)** of a KO mouse with a 4g fibrotic spleen (upper pictures) and of one secondary recipient (lower pictures). Spleen weights in primary (n=3) and secondary recipients (n=4) **(C)**. Each dot represents one mouse. The bar indicates the mean weight (WT).

Supplemental Experimental Procedures

Mice experimentation

Eight to twelve week-old WT or *p19*$^{INK4d-/-}$ mice were used as recipients for transplantation assays. Recipient mice were irradiated at lethal (11 Gy) or sublethal (10.5 Gy) doses. Cells were injected in a volume of 100 or 200 μL into the retro-orbital plexus 24 h after irradiation. 5-Fluorouracil (5-FU) or bromodeoxyuridine (BrdU) were injected intra-peritoneally in a volume of 100 μl/10 g body weight. Peripheral blood (100 μL) was collected under anesthesia with 5% isofluorane from the retro-orbital plexus into heparin-coated capillaries and suspended in 3% citrate. Nucleated cells, differential cell counts, hematocrit levels and platelet counts were determined using an automated blood counter (MS9, Melet Schloessing, Cergy-Pontoise, France). Bone marrow (BM) and spleen cells were collected post-euthanasia by carbon dioxide and processed immediately. BM cells were collected by flushing two femurs and two tibias of individual mice with PBS (1X) supplemented with 5% fetal calf serum (FCS) using a 28G needle. Cellularity was calculated using the four bones of mice. Spleen cells were obtained after grinding half a spleen and cellularity was calculated by reporting the half spleen measure to the entire spleen.

Flow Cytometry

To evaluate the distribution or to sort cells within the LSK compartment, BM cells were resuspended at 10^8 cells/mL and incubated with a lineage Lin$^-$ cocktail «biotin mouse lineage panel» against B220, GR-1, MAC-1, CD3, and TER119 (CAS number: 559971, Pharmingen, San Diego, California). Cell were subsequently stained with biotin streptavidin-APC Cy7 (CAS number: 405208, BioLegend, UK) or a cocktail of B220 APC (Clone: RA3.6B2, CAS number: 103212, BioLegend, UK), GR-1 APC (Clone: RB6.8C5, CAS number: 108412, BioLegend, UK), MAC-1 APC (Clone: M1/70, CAS number: 101212, BioLegend, UK), CD3 APC (Clone: 17A2, CAS number: 100235, BioLegend, UK) and TER119 APC (CAS

number: 116212, BioLegend, UK) with anti-mouse C-KIT-PerCP5.5 (Clone: 2B8, CAS number: 105824, BioLegend, UK), SCA-PE Cy7 (Clone: D7, CAS number: 115904, BioLegend, UK), CD150-PE (Clone: TC15-12F12.2, CAS number: 103212, BioLegend, UK), CD48-APC (Clone: HM48-1, CAS number: 103412, BioLegend, UK) or pacific blue (Clone: HM48-1, CAS number: 103418, BioLegend, UK). Hematopoietic progenitor cells were stained with streptavidin-APC Cy7, SCA-PE-Cy7, C-KIT-PE Cy5.5, CD150-APC (Clone: TC15-12F12.2, CAS number: 115910, BioLegend, UK), CD105-Pacific blue (Clone: MJ7/18, CAS number: 120412, BioLegend, UK), FCγR-PE (Clone: 93, CAS number: 101308, BioLegend, UK). Apoptotic cells were stained with Annexin V-Pacific blue antibody (CAS number: 640918, BioLegend, UK). For all experiments, specific IgG related to each antibodies were used as negative control. Flow cytometry was performed using a FACS LSR II or FACS CANTO II (BD, Mountain View, CA) and data analysis was performed with DIVA software. To sort cells, MoFlo or Influx flow cytometers (BD, Mountain View, CA) were used.

For SP staining, BM cells were resuspended at 10^8 cells/mL and stained with the APC conjugated Lin^- cocktail, PE-Cy7 conjugated SCA, and PerCP5.5 conjugated C-KIT antibodies for 30 min at 4°C. Subsequently cells were washed in cold PBS (1X) and resuspended at 10^6 cells/mL in Dulbecco modified Eagle medium (DMEM) supplemented with 5% FCS, 10 mM HEPES and stained with 5 µg/mL Hoechst 33342 (CAS number: 23491-52-3, Sigma-Aldrich, St Louis, MO) for 90 minutes at 37°C. Cells were then resuspended in cold Hanks balanced salt solution (HBSS) containing 5% FCS. Analysis of SP cells was performed on a FACS LSR II (BD, Mountain View, CA).

Ploidy of MK was performed on flushed BM cells resuspended in 2 mL of 1/1 CATCH-PBS FCS 5% media and labeled with FITC–anti-CD41 mAb after preincubation with anti-CD16/CD32 Fc(III/II) antibody. Cells were then washed and incubated in a hypotonic citrate

solution containing 50 μg/mL propidium iodide (PI) (CAS number: 25535-16-4, Sigma-Aldrich, St Louis, MO) for at least 4 h at 4°C. Ploidy level was measured on a LSR II (BD, Mountain View, CA) cytometer.

For cell cycle analysis after HU treatment, Lin^- cells were isolated and resuspended in lysis buffer (Triton 0.1%, 1 mg/mL of sodium citrate) containing RNAse (20 mg/mL) and PI (20 mg/mL).

For cell cycle analysis of HSC, total BM cells were flushed in PBS (1X), resuspended at 10^8 cells/mL and stained for 30 min on ice with a Lin^- cocktail. Cells were washed and incubated with PE-Cy7 conjugated anti-SCA1, PerCP5.5 conjugated anti-C-KIT, PE conjugated anti-CD150, APC conjugated anti-CD48 and APC-Cy7 conjugated anti-streptavidin antibodies. Cells were then washed, incubated with a cytofix-cytoperm buffer for 15 min on ice and washed twice in 1X Permwash buffer (BD Bioscience, Strasbourg, France). Cells were then incubated with FITC conjugated anti-Ki-67 (CAS number: 556026, BD Bioscience, Strasbourg, France) diluted in 1X Permwash buffer for 45 min on ice. Following this, cells were washed in 1X Permwash buffer and stained for 30 min with Hoechst 33342 at room temperature (RT) and analyzed with a MoFlo cell sorter or a LSR II cytometer (BD, Mountain View, CA). For long-term BrdU kinetic experiments, mice were injected intra-peritoneally with BrdU (1 mg/6 g body weight, Sigma-Aldrich, St Louis, MO) and were allowed to freely drink water containing BrdU (1 mg/mL) for 21 days. At days 1, 4, 8, 11 and 21, mice were sacrificed and BM was flushed and LSK and SLAM cells were stained with previously described antibodies. BrdU incorporation was evaluated by using BrdU-FITC (BrdU intracellular staining kit, BD Bioscience, Strasbourg, France) antibody and Hoechst 33342 (10 mg/mL, Sigma-Aldrich, St Louis, MO) as DNA content.

Competitive transplantation

As the genetic background of our mice (C57BL/6 x Sv129J) is not associated with a polymorphism in Ly5, the donor cells were distinguished by using lentiviruses encoding GFP or Cherry. Lin^- cells from 8 week-old mice were isolated as previously described and transduced at day 0 in MEMα media supplemented with SCF (20 ng/mL), TPO (10 ng/mL), IL3 (10 ng/mL), IL6 (10 ng/mL) and FLT3 (20 ng/mL). Lin^- cells from WT mice were transduced with a sinPRRL lentivirus encoding GFP and cells from *p19*$^{INK4d-/-}$ mice with a sinPRRL lentivirus encoding CHERRY. At day 2, cells were sorted on the Lin^-GFP^+ (WT) or $Lin^-CHERRY^+$ (*p19*$^{INK4d-/-}$) and $5x10^4$ of both Lin^-GFP^+ and $Lin^-Cherry^+$ cells were re-injected retroorbitally into sublethally irradiated WT recipient mice. The number of injected SLAM cells per mouse was calculated based on the percentage of SLAM cells within the LSK population and of LSK cells within the Lin^- population.

Histology and immunohistochemistry

Freshly collected bones were fixed in 4% paraformaldehyde and embedded in paraffin, and sections (4 μm) were stained with hematoxylin eosin and safran. For VWF immunohistochemistry, paraffin sections were processed for heat-induced antigen retrieval (citrate buffer pH 6 for 30 min) and incubated for 1 h with VWF antibody (1/200; Dako). Staining was visualized using the peroxidase/diaminobenzidine Rabbit PowerVision kit (ImmunoVision Technologies). All slides were immunostained in cover plates the same day, ensuring a perfectly standardized intensity of staining. Argentafin reticular fibers staining was performed with a standard histological staining kit (Argentafin reticular fibers Kit; Diapath). The kit detects argyrophyl reticular fibers in connective tissue. Reticular fibers argyrophyl characteristics are given by the capacity to link argental salts, which once reduced as metal silver, have a typical black stain. Nervous and reticular fibers: black; Connective: brown; Collagen: yellow. Slides were examined using a Zeiss Axiophot microscope (Carl Zeiss, Le

Pecq, France) with 2.5×1 (magnification ×2.5) or 10×/1 (magnification ×10) numeric aperture objectives.

Quantitative real-time RT-PCR (qRT-PCR)

RNA was extracted with the RNeasy micro kit (Qiagen) and reverse transcription was performed with the superscript VILO kit (Invitrogen). Primers and internal probes for qRT-PCR were designed using primer 3 software. qRT-PCR was performed with an ABI 7500 Fast real-time PCR system using SYBR Green Universal Master mix containing specific primers. The expression level of all genes was expressed relative to *ML-32*, *HPRT* and *PPIA*. As the results were similar, only those relative to *HPRT* are presented. Probes and primers used in qRT-PCR assays are listed in **Table S**. Data were analyzed with 7500 Fast system SDS software 1.3.1. All experiments were performed in duplicate.

Table S, primer list.

Primer	Sequence
p16INK4a F	CCCAACGCCCCGAACT
p16INK4a R	GAGCAGAAGAGCTGCTACGTGAA
p15INK4b F	ATCCCAACGCCCTGAACCGCT
p15INK4b R	AGTTGGGTTCTGCTCCGTGGAG
p18INK4c F	GTCAACGCTCAAAATGGATTTGGG
p18INK4c R	GGATTAGCACCTCTGAGGAGAAG
p19INK4d F	GGAGCTGGTGCATCCTGACGC
p19INK4d R	TGGCACCTTGCTTCAGGAGCTC
p21CIP1 F	TCGCTGTCTTGCACTCTGGTGT
p21CIP1 R	CCAATCTGCGCTTGGAGTGATAG
p27KIP1 F	AGCAGTGTCCAGGGATGAGGAA
p27KIP1 R	TTCTTGGGCGTCTGCTCCACAG
p57KIP2 F	AGCTGAAGGACCAGCCTCTCTC
p57KIP2 R	ACGTCGTTCGACGCCTTGTTCT
HPRT F	GCCTAAGATGAGCGCAAGTTG
HPRT R	TACTAGGCAGATGGCCACAGG
PPIA F	GGCCGATGACGAGCCC
PPIA R	TGTCTTTGGAACTTTGTCTGCAA
mL32 F	GAAACTGGCGGAAACGCA
mL32 R	GGATCTGGCCCTTGAACCTT

Treatment for myelosuppression by administration of 5-FU

To study cell cycle of LSK and SLAM cells, one simple PI injection of 5-FU at 250 mg/kg body weight was used. To analyze the survival rate of mice after the myelosuppressive treatment, 5-FU was intra-peritoneally injected on a weekly basis (150 mg/kg body weight) until the death of mice. To rule out systemic toxicity of 5-FU, WT and *p19*$^{INK4d-/-}$ mice were

reconstituted with either WT or *p19*$^{INK4d-/-}$ Lin$^-$ cells. One month after transplantation and reconstitution of the hematopoietic system, 5-FU (150 mg/kg body weight) was injected once per week for 2 weeks and animal survival rates were followed. Analysis of cell cycle and apoptosis was performed 2 days after 5-FU injection (50 mg/kg body weight) into chimeric mice two months after hematopoietic reconstitution.

Assessment of colony-forming cell (CFC) potential

To assess clonogenic potential, total BM cells were plated at a concentration of 0.5-1x10^3 cells/mL in methylcellulose medium (Methocult M3234, Stem Cell Technologies, Vancouver, Canada). Colonies derived from CFCs were scored at days 7-12 under an inverted microscope (Nikon, Japan). To determine the proliferation rate of myeloid progenitors, Lin$^-$Sca-1$^-$c-Kit$^+$ cells were sorted at one cell/well in 96-well plates and cultured in DMEMα media supplemented with 10% FCS and 50 ng/mL SCF or 20 ng/mL G-CSF. At day 7, the number of cells per colony was counted using an inverted microscope (Nikon, Japan). To measure the clonogenic potential of SLAM in 48 week-old mice, OP9/OP9Δ1 co-culture was performed. 5 x10^4 OP9/OP9Δ1 (1:1) stromal cells were plated on 96-well plates. One day after, WT or *p19*$^{INK4d-/-}$ SLAM cells of ≤ 48 week-old mice were sorted at one cell/well in the 96-well plates containing stromal cells and incubated in DMEMα + 15% FCS. Cells were maintained in culture for 21 days by changing half of the medium once per week, and colony numbers were assessed. To assess the clonogenic potential of MK-Ps, total BM and spleen cells were plated at 75x10^3 cells/mL and 150x10^3 cells/mL, respectively, in serum-free fibrin clots. MK colonies were enumerated seven days after acetylcholinesterase staining, as previously described (Long and Williams, 1981).

Cytokine arrays

After flushing BM or crushing spleen in PBS (1X), cells were centrifuged and supernatants of BM and spleen of WT and *p19*$^{INK4d-/-}$ mice were collected. TPO levels were measured using

the Mouse Thrombopoietin Quantikine ELISA Kit (R&D system). Latent and active TGFβ1 levels were measured using the Human TGFβ1 Quantikine ELISA Kit (R&D system). Levels of 40 cytokines/chemokines were measured using the Mouse Cytokine Antibody Array, Panel A (R&D system).

Oxidative stress induction

Lin^- cells were isolated and incubated in 25 cm^3 culture bottles at a density of 1×10^6 cells/mL with or without menadione (10 mM) in DMEMα supplemented 10% FBS media. After 1 h of incubation, cells were washed in HBSS (1X) and stained with the APC conjugated Lin^- cocktail, PE-Cy7 conjugated Sca1, and PerCP5.5 conjugated c-Kit antibodies for 30 min at 4°C. Briefly, to measure ROS production by flow cytometry, LSK and SLAM cells were incubated before or after oxidative stress induction with 10 μmol/mL $DCFH_2$-DA at 37°C for 15 min. Cells were resuspended in 200 μL of HBSS (1X) and analyzed using an LSR II flow cytometer (BD, Mountain View, CA).

For measurement of DNA double stranded breaks, LSKs were cytocentrifuged at 700 rpm for 7 min on L-polylysine coated slides and fixed with PFA 4% for 20 min at RT. Cells were washed with PBS (1X), permeabilized with cold ethanol 70% for 20 min on ice and washed two times with PBS (1X). Cells were then saturated for 90 min in PBS (1X)-BSA 8% and stained with primary P-H2AX (Cell signaling, Boston, USA) and secondary ALEXA-546 antibodies (Invitrogen, Saint Aubin, France). Nuclei were stained with Dapi (Sigma-Aldrich, St Louis, MO). Cells were examined using a Leica DMI 4000, SPE, laser scanning microscope (Leica, Microsystem, France) with a 63X/1.4 numeric aperture (NA) oil objective. Images were processed using Adobe Photoshop 6.0 software.

References

Long, M.W., and Williams, N. (1981). Immature Megakaryocytes in the Mouse: Morphology and quantitation by acetylcholinesterase staining. Blood *58*, 1032-1039.